Research Square

Preprints are preliminary reports that have not undergone peer review.
They should not be considered conclusive, used to inform clinical practice,
or referenced by the media as validated information.

Mind the gap: Sex-specific computational modeling reveals distinct mechanisms in bone fracture healing

Laura Lafuente-Gracia
KU Leuven
Jamie Madrigal
University of North Carolina at Chapel Hill
Pieter Ansoms
KU Leuven
Kerri-Ann Norton
Bard College
Ning Wei
Purdue University West Lafayette
Liesbet Geris
KU Leuven
Sarah L. Waters
University of Oxford
Aurélie Carlier
a.carlier@maastrichtuniversity.nl

Maastricht University

Research Article

Keywords:

Posted Date: November 11th, 2026

DOI: https://doi.org/10.21203/rs.3.rs-9558013/v1

License: This work is licensed under a Creative Commons Attribution 4.0 International License.
Read Full License

Additional Declarations: No competing interests reported.

Mind the gap: Sex-specific computational modeling reveals distinct mechanisms in bone fracture healing

Laura Lafuente-Gracia[1,2*], Jamie Madrigal[3], Pieter Ansoms[1], Kerri-Ann Norton[4], Ning Wei[5], Liesbet Geris[1,2,6,7*†], Sarah L. Waters[8*†], Aurélie Carlier[9*†]

[1]Biomechanics Section, Department of Mechanical Engineering, KU Leuven, Leuven, Belgium.
[2]Prometheus: Division of Skeletal Tissue Engineering, KU Leuven, Leuven, Belgium.
[3]Mathematics Department, University of North Carolina at Chapel Hill, Chapel Hill, North Carolina, USA.
[4]Computer Science Program, Department of Science, Mathematics, and Computing, Bard College, Annandale-on-Hudson, New York, USA.
[5]Department of Mathematics, Purdue University, West Lafayette, Indiana, USA.
[6]Skeletal Biology and Engineering Research Center, KU Leuven, Leuven, Belgium.
[7]Biomechanics Research Unit, GIGA in silico medicine, University of Liège, Liège, Belgium.
[8]Mathematical Institute, University of Oxford, Oxford, UK.
[9]Maastricht Centre for Systems Biology and Bioinformatics (MaCSBio), Maastricht University, Maastricht, The Netherlands.

*Corresponding author(s). E-mail(s): laura.lafuentegracia@kuleuven.be; liesbet.geris@kuleuven.be; sarah.waters@maths.ox.ac.uk; a.carlier@maastrichtuniversity.nl;
Contributing authors: jamiemadrigal14@gmail.com; pieter.ansoms@kuleuven.be; knorton@bard.edu; wei307@purdue.edu;
†These authors contributed equally to this work.

Abstract

This study presents the first sex-specific computational model of bone fracture healing, addressing the limited and often contradictory understanding of sex differences in this process. An existing inflammation-repair model was adapted using literature-derived sex-specific parameter values. Independent global sensitivity analysis identified several of these parameters among the main drivers of model dynamics. Due to the critical role of inflammation in fracture repair, a non-dimensional timescale analysis was used to characterize the temporal organization of early fracture healing. Two characteristic timescales common to females and males were identified, capturing fast cytokine regulation and slower cellular processes. Although this analysis did not reveal sex-dependent timescales, it provided an interpretative framework within which quantitative sex differences emerged in full-model predictions. These differences included faster macrophage activation and enhanced phagocytosis in females, leading to quicker debris clearance and stronger, more sustained inflammatory responses with elevated anti-inflammatory cytokine production. In contrast, males exhibited higher pro-inflammatory cytokine levels, a shorter inflammatory phase, and higher peaks in skeletal stem/progenitor cell and fibrocartilage densities. Despite these mechanistic differences, the model predicted comparable healing outcomes in females and males. Validation against independent *in vivo* data showed good agreement, including the predicted sex-specific differences in the fibrocartilage compartment and similar osteoblast numbers and ossification patterns between sexes. By integrating sex-specific data from diverse experimental sources, often focused on isolated subprocesses, into a unified computational framework, this work reproduces emergent, sex-specific healing dynamics consistent with experimental observations, highlighting the importance of incorporating sex-specific biology into computational models and supporting their use to advance personalized treatment strategies.

Keywords: bone fracture healing, sex differences, sex-specific modeling, computational model, inflammatory response, tissue regeneration, global sensitivity analysis

Plain English summary

Bones heal through a complex process that involves different cell types regulated by biochemical factors, ultimately leading to the formation of new tissue. Experimental studies have shown that females and males can differ in how bone fractures heal, but the biological reasons for these differences are still not fully understood. One challenge is that many studies focus on individual aspects of healing, making it difficult to understand how sex-specific differences interact across the entire healing process. In this study, we developed a computational model of bone fracture healing that explicitly accounts for biological differences between females and males. The model uses sex-specific parameter values derived from many experimental studies. Using this approach, the model predicts differences in the behavior of immune and repair cells, as well as in the biochemical factors that regulate them. Despite these differences, the predicted overall bone formation is similar between sexes. Both the sex-specific healing

trajectories and the overall healing outcomes agree well with experimental observations. By bringing together diverse experimental results into a single computational model, this work highlights the importance of considering sex as a biological variable and demonstrates how computational approaches support the development of more personalized strategies for bone fracture healing.

Highlights

- First computational model of bone fracture healing incorporating sex differences
- Literature-derived sex-specific parameterization supported by global sensitivity analysis
- Timescale and numerical analyses provide insight into healing dynamics
- Model predicts sex-specific inflammatory and repair responses
- Predictions show strong agreement with independent sex-specific *in vivo* observations

1 Introduction

Bone possesses a remarkable regenerative capacity. After a bone fracture occurs, successful healing is usually achieved within weeks. However, up to 10% of bone fractures result in a delayed- or non-healing outcome [1, 2]. Such healing complications negatively affect patients' quality of life through pain and reduced mobility [3], and also lead to increased costs. These include direct healthcare costs, such as additional surgical interventions and prolonged medication use [4], as well as indirect societal costs, such as extended work absence and caregiver burden [5]. The causes of delayed- or non-healing outcomes are multifactorial and include fracture severity, anatomical location, treatment rendered, and host factors such as sex, age, and the presence of other comorbidities [6]. Although the importance of sex differences in biological processes is becoming increasingly recognized [7], the role of sex differences in fracture healing is still poorly understood, and experimental results report contradictory findings. For example, while some authors report no significant sex differences [8], other studies suggest a sexually dimorphic inflammatory response [9–11] leading to less efficient bone healing in females [12–14] or, contrarily, in males [15]. It is thus not clear how sex disparities contribute to the emergent bone healing outcome.

Given the intricate nature of the bone healing process, which involves many interacting biological factors, computational models provide a systematic approach to understanding the impact of sex differences and supporting the design of tailored treatment strategies for both sexes. In this paper, we investigate sex differences in normal fracture healing by adapting an existing computational model, with the aim of highlighting the importance of accounting for sex-specific variation.

1.1 Normal fracture healing

Bone tissue has the unique capacity of autonomous regeneration without fibrous scar formation after most injuries. This healing process involves the coordinated participation of several cell types, regulated by a myriad of biochemical, physical, and

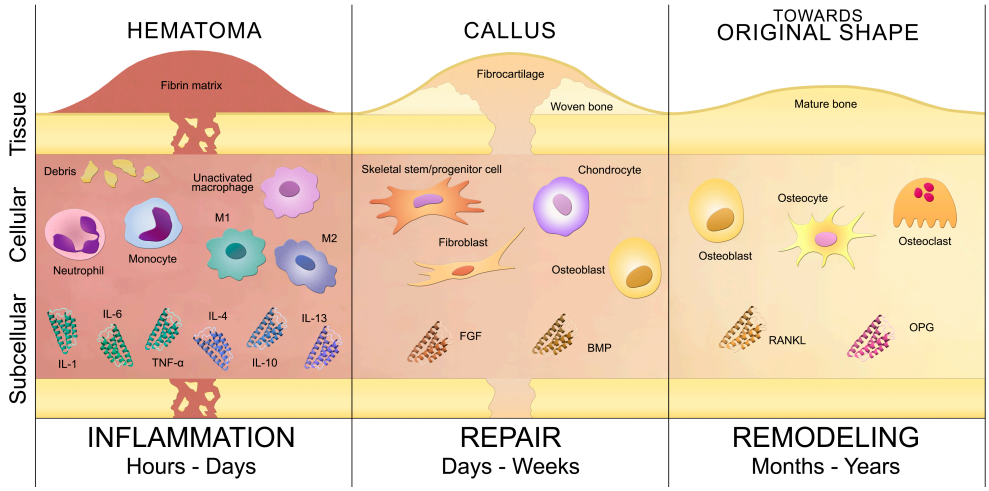


Fig. 1 Secondary bone fracture healing process. Timeline of the three overlapping healing phases (inflammation, repair, and remodeling) at tissue, cellular, and subcellular levels. Inflammation (left): hematoma formation triggers the invasion of inflammatory cells (neutrophils, monocytes, macrophages) and the release of pro-inflammatory (IL-1, IL-6, TNF-α) and anti-inflammatory (IL-4, IL-10, IL-13) cytokines. Unactivated macrophages polarize into pro-inflammatory (M1) or anti-inflammatory (M2) phenotypes. Repair (center): soft callus (fibrocartilage) and subsequent hard callus (woven bone) formation are regulated by repair cells (SSPCs, fibroblasts, chondrocytes, osteoblasts) and growth factors (FGF, BMP). Remodeling (left): hard callus is reabsorbed and replaced with mature bone by osteoblasts, osteocytes, and osteoclast, regulated by RANKL and OPG. Figure adapted from [21].

mechanical factors [16, 17]. There are two types of fracture healing, determined by the mechanical environment: primary (or direct) healing and secondary (or indirect) healing. Primary healing is less common and occurs only under conditions of absolute mechanical stability at the fracture site, which inhibits callus formation [18, 19]. By contrast, secondary healing is predominant in most clinical cases and is driven by micro-motion, or relative stability, between the bone fragments, which stimulates callus formation [18–20]. Here, we focus on secondary fracture healing, which comprises three main overlapping phases: inflammation, repair through soft and hard callus, and remodeling (Figure 1).

Following trauma, the inflammatory phase begins immediately with hematoma formation at the injury site. The hematoma acts both as a source of signaling molecules [16] and as a temporary scaffold [19], initiating the healing cascade. Tissue-resident cells, including tissue-resident macrophages, recognize the accumulation of debris from necrotic cells and damaged tissue within the hematoma and release pro-inflammatory cytokines, which contribute to the further recruitment and activation of inflammatory cells, such as neutrophils, monocytes, and macrophages [3, 17, 22, 23]. In parallel, the fibrin network formed inside the hematoma provides a provisional matrix that supports their migration to the injury site [3, 17]. Among the resident and recruited cells, macrophages display a continuum of different activation states depending on the local environment [24]. Despite this continuum, they are often grouped into two

broad polarization phenotypes: pro-inflammatory (M1) and anti-inflammatory (M2), which can switch in response to signals from the injury microenvironment throughout the healing process [24]. Macrophages remove debris and the temporary fibrin matrix through phagocytosis [17]. M1 macrophages dominate the early inflammatory phase [25] and amplify the inflammatory reaction by secreting pro-inflammatory cytokines, such as interleukin 1 and 6 (IL-1, IL-6) and tumor necrosis factor alpha (TNF-α) [23]. These cytokines typically peak within the first 24 hours after injury and recruit additional inflammatory cells and skeletal stem/progenitor cells (SSPCs) [19, 22, 23, 25]. In contrast, M2 macrophages become more prominent as healing progresses, modulating the inflammatory response and supporting tissue regeneration [25], thereby preventing excessive inflammation that could hinder fracture repair. M2 macrophages release anti-inflammatory cytokines, such as IL-4, IL-10, and IL-13, which, together with both recruited and tissue-resident SSPCs, regulate the transition from an inflammatory to a regenerative environment by promoting the polarization of macrophages toward an M2 phenotype [22, 23, 25]. This emerging pro-regenerative environment contributes to the downregulation of inflammation, as early repair cells such as SSPCs and fibroblasts begin transforming the hematoma into granulation tissue [18]. Consequently, the initial fracture hematoma and associated acute inflammatory response are generally resolved within several days to a week after injury [17, 20]. Overall, this early inflammatory phase is critical in bone healing, and any disruption during this process can significantly delay or hinder successful regeneration [3].

The subsequent progression of the repair phase depends on the mechanical environment at the fracture site [18, 19]. Under conditions of relative stability, SSPCs differentiate into chondrocytes, which produce fibrocartilage to bridge the fracture gap, forming a soft callus and stabilizing the fracture site [17–20]. As chondrocytes proliferate, they mature into hypertrophic chondrocytes, release calcium, undergo apoptosis, and then are replaced by osteoblasts [17, 19]. As a result, the soft callus calcifies and forms woven bone or hard callus through endochondral ossification [18]. While soft callus formation proceeds, SSPCs can directly differentiate into osteoblasts in mechanically stable regions near the bone ends, contributing to woven bone formation through intramembranous ossification [17]. These repair processes are regulated by various growth factors, such as fibroblast growth factor (FGF) and bone morphogenetic proteins (BMPs), which coordinate cellular behavior and tissue regeneration [26]. The hard callus formation is completed within several weeks to months after the trauma [17]. Although the hard callus provides mechanical stability, full restoration of the bone's properties is only achieved through the remodeling phase, which in humans can take several months to years to complete [17, 19, 20]. In this final phase, regulated by proteins such as receptor activator of nuclear factor kappa-B ligand (RANKL) and osteoprotegerin (OPG), the immature bone is resorbed by osteoclasts and replaced with mature bone by osteoblasts. At the same time, osteoblasts undergo apoptosis or become embedded in the bone matrix as osteocytes [17, 20].

Importantly, each step of this tightly orchestrated bone fracture healing process may be influenced by sex differences, an aspect we explore in more detail in the following section.

1.2 Sex differences in fracture healing

Recent evidence points toward a sex specific regulation of bone homeostasis and fracture healing, likely due to differences in skeleton mechanics [8, 12, 14, 27] and sex hormones [10, 12–14, 27–29]. Sex hormones also fluctuate during puberty, menopause and aging, affecting individuals differently at different life stages [27]. Due to the complexity of investigating sex differences across different stages of life, including age, day of menstrual cycle and pregnancy or lactation state, we focus this study on sex differences in young males and females of reproductive age. Gender, which is a different concept to biological sex and also influences health outcomes [28], will not be considered here.

Regardless of age and even species, females tend to show sustained or enhanced immune responses after trauma [30, 31]. Reported sex differences in immune cells include increased numbers of macrophages [15, 31, 32] with higher activation rates [30, 31, 33] and enhanced phagocytosis [15, 30, 32] in females, and larger numbers of natural killer cells in males [30]. It is not clear whether macrophage polarization is sex-dependent, as the literature reports contradictory findings [8, 15]. There are also sex differences in cytokine production: male immune cells tend to produce a greater amount of pro-inflammatory cytokines, whereas female immune cells produce higher levels of anti-inflammatory cytokines [8, 14, 15, 28, 30, 31, 34, 35]. As many of these findings are based on immune responses in general or on studies involving other tissues or in vitro models, their relevance to fracture healing remains to be confirmed. To date, few studies have investigated sex-specific inflammatory responses during fracture healing. Molitoris et al. [8], however, examined inflammatory cell populations and cytokine profiles in bone tissue and circulation to identify age- and sex-related differences during homeostasis and fracture repair in mice. In young, uninjured mice, females showed fewer M1 and M2 macrophages in bone, and reduced M1 macrophages and neutrophils in circulation compared to males. Pro-inflammatory cytokines were also lower in young females. After fracture, these sex differences were no longer observed within the callus or circulation, although a decrease in M1 macrophages within the callus was seen only in young males. The authors suggest that inflammation plays a greater role in age-related than in sex-related differences in fracture healing. Nonetheless, limitations such as analysis at a single post-fracture time point and the fracture model used indicate that subtle or early sex-specific inflammatory responses may have been missed. Altogether, the limited and sometimes inconsistent findings on sex-specific immune responses in fracture healing, along with more robust evidence from other systems, highlight the need for further investigation.

In the crosstalk between macrophages and SSPCs, cells from male mice benefited from a longer period of pro-inflammatory exposure than those from female mice, leading to increased osteogenesis in males [15]. The SSPC immunosuppressive capacity seems to be more potent in women [36, 37], but murine studies in bone tissue detected little or no differences [38, 39]. Male mice and rats have a higher quantity of (activated) SSPCs in the bone marrow [15, 37, 38, 40], leading to a significantly stronger repair response [13, 40]. The SSPC proliferation rate was found to be higher in women [37] and female mice [41], but the opposite was also reported for female rats [40]. SSPCs from male mice and rats showed stronger differentiation potential toward the

osteogenic [11, 15, 37, 38, 40, 41], chondrogenic [29, 41] and adipogenic [38] lineages. The senescence ratio of murine [40] and porcine [37] SSPCs were higher in males. The ratio of apoptosis was also higher in the SSPCs of male mice [35]. After osteogenic differentiation, murine female osteoblasts increased in number due to a higher expression of RANKL and OPG [10, 31]. No significant differences in osteoblast numbers were found between male and female mice [12]. By contrast, male mice exhibited significantly increased osteoclast numbers and activity in the fracture callus [12, 14], although the opposite was also reported: more osteoclasts at the fracture site in female mice [9]. At the tissue level, male mice developed significantly more cartilage and less fibrous tissue in the fracture callus than females, with no significant difference in callus size, indicating faster cartilaginous callus formation [12]. Similarly, human SSPC-derived organoids showed greater cartilage production in male than in female constructs [42]. Male mice displayed quicker and more robust bone formation due to faster endochondral ossification [10, 12, 29]. Consequently, male mice presented more mature bone in the fracture callus than female mice at the same time point, indicating a faster fracture healing process [12]. However, the opposite was also reported: after an induced femur fracture, female mice exhibited higher systemic bone formation than male mice [15]. Sex differences have also been reported in bone remodeling and turnover. However, although the literature suggests sex-dependent regulation of remodeling processes [43, 44], direct evidence for sex-specific rates of woven bone resorption during fracture healing was not identified. Together, these findings suggest that, while sex-based differences during bone healing exist, they vary depending on species and, most likely, experimental conditions, resulting in a complex and sometimes contradictory research landscape.

Finally, clinical indications suggest sex differences in pathological cases of fracture healing: women present an increased risk for atrophic non-unions, which involve insufficient healing activity and minimal or no callus formation, while men are more prone to hypertrophic non-unions, characterized by excessive callus formation and inadequate stability [12]. Although it has been suggested that the risk of non-union varies with sex, with men exhibiting a higher risk [1, 45], systematic reviews have found that sex as a risk factor for non-union is not statistically significant [46–48].

1.3 Objective of this study

The objective of this study is to investigate sex differences in normal fracture healing through computational modeling. To date, various computational fracture healing models have been developed. For extensive reviews, the reader is referred to [21, 49–55]. In recent years, these models have been extended to include the inflammatory response during fracture healing [56–60]. However, to the best of our knowledge, there are no computational models of sex-dependent fracture healing. Although delayed and non-union fractures are clinically significant, they arise from a complex interplay of biological, mechanical, and systemic factors that remain incompletely understood. Since no sex-specific models currently exist, we focus first on characterizing potential sex differences under conditions of normal healing, with the aim of providing the necessary foundation for future studies that may address pathological scenarios.

The remainder of this paper is organized as follows. Section 2 presents the computational framework used to investigate sex differences in bone fracture healing. First, we revisit the macrophage-mediated model of Trejo et al. [57], which captures the inflammatory and repair phases of healing and is adopted here without structural changes but with updated parameter values. We refer to this as the *full* model. Second, we perform a variance-based global sensitivity analysis using Sobol indices. Third, we introduce the sex-specific parameterization based on the literature review of sex differences presented in Section 1.2. Fourth, given the central role of the inflammatory phase, we focus on the corresponding equations and non-dimensionalize them to identify the underlying timescales and provide mechanistic insight into the system dynamics. We refer to this as the *early-healing* (EH) submodel. Finally, model implementation details are provided. Section 3 first presents the results of the global sensitivity analysis and then the sex-specific healing dynamics predicted by the model, including both the timescale analysis and numerical simulations. While overall healing trends are similar for both sexes, the model reveals notable differences in underlying biological processes that align with the literature. These predictions are then validated against independent *in vivo* data, showing good agreement. Section 4 interprets the main findings, contextualizing the observed sex differences within existing biological evidence. It also highlights the strengths and potential of computational modeling for studying fracture healing across sexes, before concluding with a discussion of the limitations of the study and directions for future research. Finally, Section 6 provides a concise summary of the key contributions and implications of this study.

2 Computational model

Sex differences in fracture healing are suggested to be present from the inflammatory phase onward; therefore, any computational model aimed at investigating how sex differences influence the healing process should incorporate this phase. Among the limited options available in the literature, we selected the macrophage-mediated model of Trejo et al. [57]. This model was chosen for several reasons. First, it describes the temporal dynamics of fracture healing from the first post-fracture days (PFDs) through to the completion of hard callus formation, making it suitable for exploring sex differences during both the inflammatory and repair phases. Second, the ordinary differential equation (ODE) framework allows biologically motivated sex differences to be incorporated through parameter modifications while preserving the underlying mechanistic structure. Third, the ODE model supports a timescale-based reduction, resulting in a simplified version that highlights the underlying biological processes underpinning the early-healing stage, as detailed in Section 2.4.

2.1 Model equations

Here, we briefly outline the model equations of Trejo et al., which describe the inflammatory and repair phases; for a detailed explanation, the reader is referred to [57]. The model consists of ten ODEs which describe the temporal evolution of the average densities of debris (D), unactivated macrophages (M_0), pro-inflammatory macrophages (M_1), anti-inflammatory macrophages (M_2), skeletal stem/progenitor cells (SSPCs,

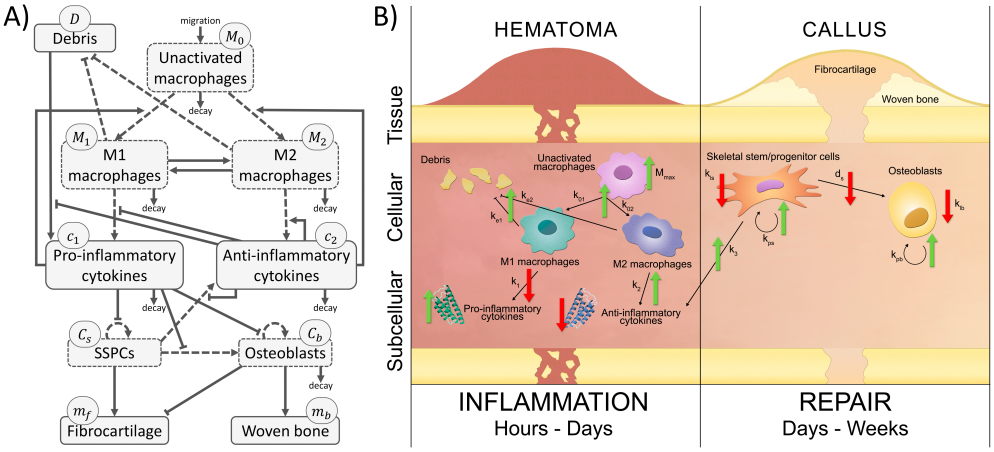


Fig. 2 Overview of the sex-specific model of bone fracture healing. A) Schematic representation of the ordinary differential equation (ODE) model, illustrating interactions among its biological entities. Cells with dashed outlines have sex-specific maximal densities, and dashed arrows represent interactions governed by sex-specific parameters (see Section 2.3). Arrowheads denote activation, and flat arrowheads indicate inhibition. Adapted from [57]. B) Illustration of the biological processes captured by the model. Interactions with sex-specific parameters are explicitly shown. Green and red arrows indicate, respectively, up- and down-regulation of female parameters regarding the male parameter set (see Table 3).

C_s), osteoblasts (C_b), fibrocartilage or soft callus (m_c), and woven bone or hard callus (m_b), together with the average concentrations of pro-inflammatory (c_1) and anti-inflammatory cytokines (c_2).

The system of ODEs captures the acute inflammatory response, in which debris is cleared by macrophages; the crosstalk between macrophages and SSPCs, which initiates the repair response; and the formation of soft and hard callus, which ultimately leads to bone repair. The cellular functions are regulated by pro- and anti-inflammatory cytokines, both modeled as a cocktail, that is: the action of several types of cytokines is lumped together in the c_1 and c_2 variables. SSPCs and osteoblasts are assumed to produce, respectively, fibrocartilage and woven bone. This is a simplified representation of the soft and hard callus formation that constitutes the outcome of the healing process. These and other interactions are illustrated in Fig. 2A.

The ODE system is described by Equations (1)–(10). Although the main phases of bone fracture healing (depicted in Fig. 1) are interconnected, Equations (1)–(6) primarily describe inflammation, while Equations (7)–(10) focus on repair. Equation (7) serves as the transition between these two phases, representing a pro-regenerative state. As described in Section 1.1, the presence of M_1 macrophages and pro-inflammatory cytokines (c_1) indicates acute inflammation, while the presence of M_2 macrophages and anti-inflammatory cytokines (c_2) reflects the resolution of the inflammatory response. We therefore consider that inflammation is taking place when any of the variables M_1, M_2, c_1, or c_2, described by Equations (3)–(6), exhibit positive values.

$$\frac{dD}{dt} = -\underbrace{R_D(k_{e1}M_1 + k_{e2}M_2)}_{\text{removal by phagocytosis}} \tag{1}$$

$$\frac{dM_0}{dt} = \underbrace{R_M D}_{\text{migration}} - \underbrace{G_1 M_0}_{\text{M1 polarization}} - \underbrace{G_2 M_0}_{\text{M2 polarization}} - \underbrace{d_0 M_0}_{\text{apoptosis}} \tag{2}$$

$$\frac{dM_1}{dt} = \underbrace{G_1 M_0}_{\text{polarization}} + \underbrace{k_{21}M_2 - k_{12}M_1}_{\text{phenotype change}} - \underbrace{d_1 M_1}_{\text{apoptosis}} \tag{3}$$

$$\frac{dM_2}{dt} = \underbrace{G_2 M_0}_{\text{polarization}} + \underbrace{k_{12}M_1 - k_{21}M_2}_{\text{phenotype change}} - \underbrace{d_2 M_2}_{\text{apoptosis}} \tag{4}$$

$$\frac{dc_1}{dt} = \underbrace{H_1(k_0 D + k_1 M_1)}_{\text{production}} - \underbrace{d_{c1} c_1}_{\text{decay}} \tag{5}$$

$$\frac{dc_2}{dt} = \underbrace{H_2(k_2 M_2 + k_3 C_s)}_{\text{production}} - \underbrace{d_{c2} c_2}_{\text{decay}} \tag{6}$$

$$\frac{dC_s}{dt} = \underbrace{A_s C_s(1 - \frac{C_s}{k_{ls}})}_{\text{proliferation}} - \underbrace{F_1 C_s}_{\substack{\text{osteogenic} \\ \text{differentiation}}} \tag{7}$$

$$\frac{dC_b}{dt} = \underbrace{A_b C_b(1 - \frac{C_b}{k_{lb}})}_{\text{proliferation}} + \underbrace{F_1 C_s}_{\substack{\text{osteogenic} \\ \text{differentiation}}} - \underbrace{d_b C_b}_{\substack{\text{osteocytic} \\ \text{differentiation}}} \tag{8}$$

$$\frac{dm_c}{dt} = \underbrace{(p_{cs} - q_{cd1} m_c) C_s}_{\text{production}} - \underbrace{q_{cd2} m_c C_b}_{\text{resorption}} \tag{9}$$

$$\frac{dm_b}{dt} = \underbrace{(p_{bs} - q_{bd} m_b) C_b}_{\text{production}} \tag{10}$$

This ODE system is complemented by the following initial conditions:

$$\left.\begin{gathered} D(0) = 5 \times 10^7 \text{ cells/mL},\ M_0(0) = 4000 \text{ cells/mL},\ M_1(0) = 0 \text{ cells/mL}, \\ M_2(0) = 0 \text{ cells/mL},\ c_1(0) = 1 \text{ ng/mL},\ c_2(0) = 0 \text{ ng/mL}, \\ C_s(0) = 1000 \text{ cells/mL},\ C_b(0) = 0 \text{ g/mL},\ m_c(0) = 0 \text{ g/mL},\ m_b(0) = 0 \text{ g/mL} \end{gathered}\right\} \tag{11}$$

The non-zero initial condition of debris (D) accounts for the accumulation of debris from necrotic cells and damaged tissue resulting from the bone fracture event. This debris accumulation immediately triggers the release of pro-inflammatory cytokines, which is reflected in the non-zero initial condition of c_1. The non-zero initial condition for unactivated macrophages (M_0) corresponds to macrophages present at the

injury site at the onset of the inflammatory response, including both tissue-resident macrophages and early-recruited monocyte-derived macrophages. Additionally, the non-zero initial condition of SSPCs (C_s) represents the presence of tissue-resident SSPCs. All other variables are assumed to have zero initial conditions: M_1, M_2, c_2, and m_c are not directly influenced by the fracture event. The zero initial condition of m_b represents the lack of bone tissue due to the fracture.

The ODE system given by Equations (1)–(10) features both constant parameters and functional forms. Functional forms, represented with uppercase letters (e.g. R_D), are used to capture non-constant rates and described in Table 1. Constant parameters, represented with lower case letters (e.g. k_{e_1}), are taken from [57] and described in Table 2. For some parameters, [57] provided a range of values. In this study, specific values within those ranges were selected for each parameter.

Table 1 Functional forms in Equations (1-10). The forms R_D, G_1 and G_2 are modeled by a Hill Type II function. The rate R_M accounts for maximal number of cells and maximal migration rate. The terms H_1 and H_2 are a function of c_2, modeling its inhibitory effects. The rates A_s, F_1 and A_b are a function of c_1, modeling its inhibitory effects.

Functional form	Description
$R_D = \frac{D}{a_{ed}+D}$	Debris removal rate
$R_M = k_{max}(1 - \frac{M_0+M_1+M_2}{M_{max}})$	M_0 migration rate
$G_1 = \frac{k_{01}c_1}{a_{01}+c_1}$	Polarization rate of M_0 into M_1
$G_2 = \frac{k_{02}c_2}{a_{02}+c_2}$	Polarization rate of M_0 into M_2
$H_1 = \frac{a_{12}}{a_{12}+c_2}$	Inhibition rate of c_1 by c_2 concentration
$H_2 = \frac{a_{22}}{a_{22}+c_2}$	Self-inhibition rate of c_2
$A_s = k_{ps}\frac{a_{ps}^2+a_{ps_1}c_1}{a_{ps}^2+c_1^2}$	SSPC proliferation rate
$F_1 = \frac{d_s a_{sb_1}}{a_{sb_1}+c_1}$	Differentiation rate of SSPCs into osteoblasts
$A_b = \frac{k_{pb}a_{pb}}{a_{pb}+c_1}$	Osteoblast proliferation rate

2.2 Sensitivity analysis

The model described in Section 2.1 comprises 37 parameters. To investigate how parameter uncertainty affects model predictions and gain insight into the model dynamics, a variance-based global sensitivity analysis was performed on the baseline parameter set presented in Table 2. The Sobol method [63, 64] was selected because it explores the entire parameter space and explicitly accounts for parameter interactions.

Parameter ranges were defined by uniformly varying each parameter by ±50% relative to its baseline value. This perturbation range was chosen based on the quantitative sex differences reported in the literature (Section 1.2). Across the studies reviewed, the average magnitude of the reported differences was approximately 50%, supporting the use of a symmetric ±50% perturbation range (Table S1). To evaluate the effect of

Table 2 Baseline parameter values with descriptions and units. Some parameter values were defined by a range in the model by Trejo et al. [57]. Here, a specific value was chosen by estimating it or by checking additional references. These values constitute the male parameter set.

Parameter	Description	Value	Reference
k_{e_1}	Debris removal rate by M_1	12 /day	Informed by [57]
k_{e_2}	Debris removal rate by M_2	24 /day	Informed by [57]
a_{ed}	Half-saturation of debris	4.71×10^6 cells/mL	[57]
k_{max}	Maximal macrophage migration rate	0.015 /day	[57, 61]
M_{max}	Maximal macrophage density	1×10^6 cells/mL	Informed by [57]
k_{01}	Activation rate of M_0 to M_1	0.611 /day	[57, 61]
k_{02}	Activation rate of M_0 to M_2	0.0836 /day	[61]
a_{01}	Half-saturation of c_1 to activate M_1	0.01 ng/mL	[57]
a_{02}	Half-saturation of c_2 to activate M_2	0.005 ng/mL	[57]
k_{12}	Transition rate from M_1 to M_2	0.075 /day	[57, 62]
k_{21}	Transition rate from M_2 to M_1	0.05 /day	[57, 62]
d_0	Apoptosis rate of M_0	0.156 /day	[57, 61]
d_1	Apoptosis rate of M_1	0.121 /day	[57, 61]
d_2	Apoptosis rate of M_2	0.163 /day	[57, 61]
k_0	Secretion rate of c_1 by debris	5×10^{-7} ng/(cells × day)	Informed by [57]
k_1	Secretion rate of c_1 by M_1	8.3×10^{-6} ng/(cells × day)	[57]
k_2	Secretion rate of c_2 by M_2	3.72×10^{-6} ng/(cells × day)	[57]
k_3	Secretion rate of c_2 by C_s	8×10^{-6} ng/(cells × day)	Section 6.1 in [57]
d_{c_1}	Decay rate of c_1	12.79 /day	Informed by [57]
d_{c_2}	Decay rate of c_2	4.632 /day	Informed by [57]
a_{12}	Effectiveness of c_2 inhibition of c_1 synthesis	0.025 ng/mL	[57]
a_{22}	Effectiveness of c_2 inhibition of c_2 synthesis	0.1 ng/mL	[57]
a_{ps}	Effectiveness of c_1 inhibition of C_s proliferation	3.162 ng/mL	[57]
a_{sb_1}	Effectiveness of c_1 inhibition of C_s differentiation	0.1 ng/mL	[57]
a_{pb}	Effectiveness of c_1 inhibition of C_b proliferation	10 ng/mL	[57]
a_{ps_1}	Constant enhancement of c_1 to C_s proliferation	20 ng/mL	Estimated
k_{ps}	C_s proliferation rate	0.5 /day	[57]
k_{ls}	Maximal C_s density	1×10^6 cells/mL	[57]
d_s	Differentiation rate of C_s into C_b	1 /day	[57]
k_{pb}	C_b proliferation rate	0.2202 /day	[57]
k_{lb}	Maximal C_b density	1×10^6 cells/mL	[57]
d_b	Differentiation rate of C_b into osteocytes	0.15 /day	[57]
p_{cs}	Fibrocartilage synthesis rate	3×10^{-6} g/(cells × day)	[57]
q_{cd_1}	Fibrocartilage degradation rate	3×10^{-6} mL/(cells × day)	[57]
q_{cd_2}	Fibrocartilage degradation rate by osteoclasts	0.2×10^{-6} mL/(cells × day)	[57]
p_{bs}	Woven bone synthesis rate	5×10^{-8} g/(cells × day)	[57]
q_{bd}	Woven bone degradation rate	5×10^{-8} mL/(cells × day)	[57]

these perturbations across the fracture healing process, we considered the outcome of eight specific variables: M_1, M_2, c_1, c_2, C_s, C_b, m_f, and m_b, as these capture events across both the inflammatory and repair stages. The peak value (i.e. the maximum value achieved during the simulated days) was recorded for all variables. In addition, the time-to-peak was evaluated for all variables except woven bone (m_b), which was excluded because its maximum was always reached at the final simulation time point. This resulted in fifteen output metrics for the sensitivity analysis.

The Sobol method [63, 64] quantifies the contribution of input parameter variability to the variance of model outputs. To assess this contribution, first-order (S_i) and

total-effect (S_{T_i}) sensitivity indices were computed for each parameter and output metric. The first-order index measures the direct contribution of a parameter to output variability, whereas the total-effect index includes both direct effects and all interaction effects involving that parameter. Contributions arising from parameter interactions were then estimated by the difference $S_{T_i} - S_i$. This approach enables identification of influential parameters and quantification of the role of parameter interactions in shaping model predictions.

To facilitate comparison across outputs, parameters were ranked according to their total-effect sensitivity index for each output metric. To ensure numerical convergence of the sensitivity indices, the analysis was repeated for increasing sample sizes $N = 2^6, \ldots, 2^{13}$. Convergence was assessed by comparing the total-effect indices obtained for consecutive sample sizes, and $N = 2^{13} = 8192$ was selected for the final sensitivity analysis. Selected results are presented in Section 3.1, with additional data reported in Section S1 of the Supplementary material.

2.3 Literature-guided sex-specific parameterization

To explore the role of sex differences in bone fracture healing, we parameterized the macrophage-mediated model of Trejo et al. [57] with sex-specific values. We assumed that the baseline parameter values, shown in Table 2, constitute the male parameter set. The female parameter set was generated by comparing each parameter with the sex-specific evidence reported in Section 1.2. Note that this literature review was conducted at the level of the model variables. That is, since the model represents cytokines through the aggregate variables c_1 (pro-inflammatory cytokines) and c_2 (anti-inflammatory cytokines), the literature review and parameter mapping were performed at the level of these aggregate representations rather than individual cytokines.

The baseline parameterization from Trejo et al. [57] was derived from murine fracture-healing data. However, as no single species provides comprehensive experimental coverage across all healing stages, a hybrid calibration strategy was adopted, justified by the conserved bone regeneration processes between mice and humans [65, 66]. Additionally, the *in vivo* dataset reported by Haffner-Luntzer et al. [12] was used as an independent dataset for model validation and was therefore not considered when deriving sex-specific parameter values.

Sex-specific evidence was evaluated for each parameter (see Table S4). Parameters were modified only when the literature provided sufficiently consistent evidence that could be directly mapped to the underlying biological process represented in the model. Parameters were left unchanged when findings were contradictory, when no rationale existed for prioritizing one source over another, or when the reported sex differences could not be translated into the model formulation. When contradictory evidence from multiple species was available, greater weight was given to human studies because of their greater clinical relevance. As a result, 13 parameters (35% of all model parameters) were assigned sex-specific values. These are summarized in Table 3 and illustrated by Fig. 2B.

The literature study informed the direction of the parameter modifications, whereas their magnitude was determined through model calibration. Since quantitative sex-specific differences were often unavailable or heterogeneous across studies, the perturbation range explored in the global sensitivity analysis served as the initial calibration range. Calibration against the literature-derived sex-specific observations summarized in Table 3 supported modifications of ±50% for inflammation-related parameters and ±25% for repair-related parameters. Further details are provided in Section S2 of the Supplementary material.

Table 3 Changes introduced to create the female parameter set, expressed as the relative percentage change from male values. The remaining parameters kept their original values, given in Table 2. The direction of each modification was informed by the literature, while the final modification magnitude was determined through calibration against the literature-derived sex-specific observations.

Biological agent	Biological event	Parameter	Change	Female value	Reference
Macrophages	Number ↑	M_{max}	+50%	1.5×10^6 cells/mL	[15, 31, 32]
	Activation ↑	k_{01}	+50%	0.9165 /day	[30, 33]
		k_{02}	+50%	0.1254 /day	
	Phagocytic capacity ↑	k_{e_1}	+50%	18 /day	[30, 32]
		k_{e_2}	+50%	36 /day	
	c_1 production ↓	k_1	-50%	4.15×10^{-6} ng/(cells × day)	[8, 14, 15, 28, 30, 31, 34, 35]
	c_2 production ↑	k_2	+50%	5.58×10^{-6} ng/(cells × day)	
SSPCs	Number ↓	k_{ls}	-25%	7.5×10^5 cells/mL	[13, 15, 37, 38, 40]
	Immunosuppression ↑	k_3	+50%	1.2×10^{-5} ng/(cells × day)	[36, 37]
	Proliferation ↑	k_{ps}	+25%	0.625 /day	[37, 41]
	Osteogenic differentiation ↓	d_s	-25%	0.75 /day	[11, 15, 37, 38, 40, 41]
Osteoblasts	Number ↓	k_{lb}	-25%	7.5×10^5 cells/mL	[13, 15, 37, 38, 40]
	Proliferation ↑	k_{pb}	+25%	0.2752 /day	[31]

The greater amount of macrophages [15, 31, 32] with higher activation [30, 31, 33] and enhanced phagocytosis [15, 30, 32] in females was incorporated into the model by up-regulating, respectively, the parameters M_{max}, k_{e_1} and k_{e_2}, and k_{01} and k_{02}. The cytokine production trend observed experimentally [8, 14, 15, 28, 30, 31, 34, 35] was implemented by down-regulating the c_1 production (parameter k_1) and up-regulating the c_2 production (parameter k_2) by macrophages. Although the literature is inconsistent regarding the higher immunosuppression of female SSPCs, we chose to implement it by up-regulating the parameter k_3 as the two studies supporting this observation used clinical data [36, 37]. Moreover, studies using pre-clinical data [38, 39] reported little differences, but not opposite findings. These parameters, involved in the inflammatory response and macrophage-SSPC crosstalk, were up- or down-regulated by ±50%.

The lower number of SSPCs in females [13, 15, 37, 38, 40] was implemented by down-regulating the maximal SSPC density k_{ls}. We chose this approach over a sex-specific initial condition because the reported sex differences concern the quantity of activated SSPCs in the bone marrow [15, 37, 38], which represents the pool of cells available to contribute to the healing process, rather than the number of SSPCs already present at the fracture site at the start of healing. Since the total number of SSPCs determines the total number of osteoblasts in the model, we down-regulated their maximal density k_{lb} accordingly. The faster SSPC proliferation reported in women [37] and female mice [41] was implemented by up-regulating the parameter k_{ps}. Although the opposite finding was reported for female rats [40], greater weight was given to the human evidence. Similarly, the higher number of female osteoblasts reported after osteogenic differentiation [10, 31] was implemented by up-regulating the osteoblast proliferation rate k_{pb}. Finally, to incorporate the weaker osteogenic differentiation of female SSPCs [11, 15, 37, 38, 40, 41] we down-regulated the parameter d_s. These parameters, involved in the repair response, were modified by $\pm 25\%$.

2.4 Early-healing submodel

The sensitivity analysis and accompanying literature review identified sex-specific parameters that characterize the underlying processes involved in bone fracture healing. As the literature review in Section 1.1 indicates, the early inflammatory phase is critical in bone healing [3]. Furthermore, we will show in Section 3.3 that simulations of the full model equations reveal the greatest sex differences in SSPCs and not in bone density (Fig. 7). Motivated by these observations, we focus our attention here on the dynamics of the system during the inflammation phase and the subsequent pro-regenerative transition, captured by Equations (1)–(7), subject to appropriate initial conditions given in Equation (11). We refer to this system as the *early-healing* (EH) submodel and perform a timescale analysis to derive a set of reduced models that capture the mechanisms driving the system while retaining the essential biology.

The EH submodel dynamics are governed by an interplay of processes with specific characteristic timescales, such as cytokine secretion by macrophages, debris clearance by pro-inflammatory macrophages, and migration of unactivated macrophages to the injury site. The parameters in Table 2 reveal that these characteristic timescales fall within one of two disparate timescales: a fast timescale in which the cytokine concentrations rapidly evolve from their initial values while the cell and debris densities remain close to their initial values, and a slower timescale in which the debris and cell population densities evolve from their initial values and the cytokine concentrations are quasi-steady.

To formally interrogate the dynamics of the EH submodel, we first non-dimensionalize Equations (1)–(7), together with their initial conditions, and identify the resulting dimensionless parameters. This process results in the dimensionless variables being of comparable size, and the relative importance of the underlying processes being captured through the size of the dimensionless parameters. Of particular relevance here are the dimensionless parameters that represent timescale ratios, as the disparity in biological timescales -fast cytokine dynamics versus much slower debris and cell dynamics- results in a subset of these ratios being asymptotically small. We

subsequently exploit this disparity in timescales to derive reduced models that retain the dominant processes on each of the two timescales and thereby provide insights into the progression of bone fracture healing through the key stages of inflammation and the pro-regenerative transition. Furthermore, non-dimensionalization also determines whether the dependencies appearing in the functional forms given in Table 1 are significant or could potentially be neglected.

2.4.1 Model reduction

We non-dimensionalize as follows:

$$\begin{aligned} \tilde{t} = k_{02}\, t, \qquad \tilde{D} = \frac{D}{D_0}, \qquad \left(\tilde{M}_0, \tilde{M}_1, \tilde{M}_2\right) &= \frac{1}{M_{\max}} \left(M_0, M_1, M_2\right), \\ \tilde{c}_1 = \frac{c_1}{[c_1]}, \quad \tilde{c}_2 = \frac{c_2}{[c_2]}, \quad \tilde{C}_s &= \frac{C_s}{[C_s]}, \end{aligned} \tag{12}$$

where $[c_1]$, $[c_2]$ and $[C_s]$ represent the typical concentrations of c_1, c_2, and C_s, respectively, and tildes denote dimensionless variables. Time is non-dimensionalized using the activation timescale of anti-inflammatory macrophages, $1/k_{02}$, which marks the transition from inflammation to a pro-regenerative environment and provides a biologically appropriate reference timescale for the early-healing dynamics. For the parameter values used here, this corresponds to approximately 12 days (see Table 2). Debris is non-dimensionalized with respect to its initial level, so that $D_0 = D(0)$. The macrophage populations are non-dimensionalized on the maximal macrophage density M_{max}. The SSPC population scale is chosen to be 10^5 cells/mL. Although the maximal SSPC density is 10^6 cells/mL, the population remains well below this value during healing (see Section 3.3). This scaling therefore ensures that the dimensionless SSPC density remains of order one. We choose $[c_1] = k_1 M_{max}/d_{c_1}$ and $[c_2] = k_2 M_{max}/d_{c_2}$, which is determined by balancing cytokine production by pro-inflammatory macrophages with the cytokine decay rate; see Equations (5) and (6).

The dimensionless governing equations, corresponding to Equations (1)–(7), are then:

$$\varepsilon_D \frac{d\tilde{D}}{d\tilde{t}} = -\frac{\tilde{D}}{\tilde{a}_{ed} + \tilde{D}} \left(\tilde{M}_1 + \frac{k_{e_2}}{k_{e_1}} \tilde{M}_2\right) \tag{13}$$

$$\varepsilon_{M_0} \frac{d\tilde{M}_0}{d\tilde{t}} = \left(1 - (\tilde{M}_0 + \tilde{M}_1 + \tilde{M}_2)\right) \tilde{D} - \tilde{k}_{01} \frac{\tilde{c}_1}{\tilde{a}_{01} + \tilde{c}_1} \tilde{M}_0 - \varepsilon_{M_0} \frac{\tilde{c}_2}{\tilde{a}_{02} + \tilde{c}_2} \tilde{M}_0 - \tilde{d}_0 \tilde{M}_0 \tag{14}$$

$$\varepsilon_{M_1} \frac{d\tilde{M}_1}{d\tilde{t}} = \frac{\tilde{c}_1}{\tilde{a}_{01} + \tilde{c}_1} \tilde{M}_0 + \frac{k_{21}}{k_{01}} \tilde{M}_2 - \frac{1}{k_{01}} \left(k_{12} + d_1\right) \tilde{M}_1 \tag{15}$$

$$\frac{d\tilde{M}_2}{d\tilde{t}} = \frac{\tilde{c}_2}{\tilde{a}_{02} + \tilde{c}_2} \tilde{M}_0 + \frac{k_{12}}{k_{02}} \tilde{M}_1 - \frac{1}{k_{02}} (k_{21} + d_2) \tilde{M}_2 \tag{16}$$

$$\varepsilon_{c_1}\frac{d\tilde{c}_1}{d\tilde{t}} = \frac{\tilde{a}_{12}}{\tilde{a}_{12}+\tilde{c}_2}\left(\tilde{k}_0\tilde{D}+\tilde{M}_1\right)-\tilde{c}_1 \tag{17}$$

$$\varepsilon_{c_2}\frac{d\tilde{c}_2}{d\tilde{t}} = \frac{\tilde{a}_{22}}{\tilde{a}_{22}+\tilde{c}_2}\left(\tilde{M}_2+\tilde{k}_3\tilde{C}_s\right)-\tilde{c}_2 \tag{18}$$

$$\varepsilon_{C_S}\frac{d\tilde{C}_s}{d\tilde{t}} = \left(\frac{\tilde{a}_{ps}^2+\tilde{a}_{ps_1}\tilde{c}_1}{\tilde{a}_{ps}^2+\tilde{c}_1^2}\right)\tilde{C}_s\left(1-\frac{[C_s]}{k_{ls}}\tilde{C}_s\right)-\frac{d_s}{k_{ps}}\frac{\tilde{a}_{sb_1}}{\tilde{a}_{sb_1}+\tilde{c}_1}\tilde{C}_s \tag{19}$$

Equations (13)–(19) are solved subject to the dimensionless version of the initial conditions given in Equation (11). The dimensionless initial conditions common to both the male and female cases are $\tilde{D}=1,\ \tilde{M}_1=0,\ \tilde{M}_2=0,\ \tilde{c}_2=0$, and $\tilde{C}_s=10^{-1}$. However, as the male and female versions of M_{max} and k_1 differ, the dimensionless initial conditions for the unactivated macrophages and the pro-inflammatory cytokines are $\tilde{M}_0=4\times10^{-3}$ and $\tilde{c}_1=1.5$ in the male model, and $\tilde{M}_0=2.7\times10^{-3}$ and $\tilde{c}_1=2.05$ in the female model.

The parameters $\varepsilon_D, \varepsilon_{M_0}, \varepsilon_{M_1}, \varepsilon_{c_1}, \varepsilon_{c_2}$, and ε_{C_s} appearing on the left-hand sides of Equations (13)–(19) are timescales normalized with respect to our representative timescale, which is the activation timescale of anti-inflammatory macrophages (see Equation (12)). These normalized timescales capture the following processes: debris clearance due to phagocytosis by pro-inflammatory macrophages ($\varepsilon_D = D_0k_{02}/(k_{e_1}M_{max})$, Equation (13)); migration of unactivated macrophages to the injury site ($\varepsilon_{M_0} = k_{02}M_{max}/(k_{max}D_0)$, Equation (14)); activation of pro-inflammatory macrophages ($\varepsilon_{M_1} = k_{02}/k_{01}$, Equation (15)); cytokine decay ($\varepsilon_{c_1} = k_{02}/d_{c_1}$ and $\varepsilon_{c_2} = k_{02}/d_{c_2}$, Equations (17) and (18)); and SSPC proliferation ($\varepsilon_{C_s} = k_{02}/k_{ps}$, Equation (19)). Equations (13)–(19) also contain several additional dimensionless parameters, indicated by tildes, that are defined in Table 4, alongside their representative male and female values.

We analyze the two parameter sets for male and female using values from Table 4. Note that all the dimensionless parameter groupings appearing on the right-hand sides of Equations (13)–(19) are at most $O(1)$, confirming that the chosen scaling appropriately balances the terms in the system. The normalized timescales for the male (*female*) cases are:

$$\begin{gathered}\varepsilon_D = 0.35\ (0.23),\ \varepsilon_{M_0} = 0.11\ (0.25),\ \varepsilon_{M_1} = 0.14(0.14),\\ \varepsilon_{c_1} = 7\times10^{-3}\ (9.8\times10^{-3}),\ \varepsilon_{c_2} = 1.8\times10^{-2}\ (2.7\times10^{-2}),\ \varepsilon_{C_s} = 0.17\ (0.2).\end{gathered} \tag{20}$$

These parameters are $O(10^{-2})$ or $O(1)$, revealing that, in both the male and female cases, the system dynamics occur over two distinct timescales: a short one (hours) and a long one (days to weeks). Since we only consider processes up to C_s, the long timescale is relative and reflects the slower behavior of the early healing process, excluding the subsequent callus formation stage. The short timescale captures the dynamics of the cytokine concentrations ($\tilde{c}_1$ and $\tilde{c}_2$), while the long timescale captures the dynamic interplay between debris ($\tilde{D}$), unactivated, pro-inflammatory, and anti-inflammatory macrophages ($\tilde{M}_0$, $\tilde{M}_1$, and $\tilde{M}_2$), and SSPCs (C_s). While it might be argued that ε_D, ε_{M_0}, ε_{M_1}, and ε_{C_s} are $O(10^{-1})$, these values are not sufficiently small

Table 4 Non-dimensional parameter definitions and values for the male and female cases. All timescales are normalized using the activation timescale of anti-inflammatory macrophages, $T = 1/k_{02} \approx 12$ days.

Non-dimensional parameter	Male value	Female value
$\tilde{a}_{ed} = \frac{a_{ed}}{D_0}$	9.4×10^{-2}	9.4×10^{-2}
$\tilde{k}_{01} = \frac{k_{01} M_{max}}{k_{max} D_0}$	0.81	1.83
$\tilde{d}_0 = \frac{d_0 M_{max}}{D_0 k_{max}}$	0.21	0.31
$\tilde{k}_0 = \frac{k_0 D_0}{k_1 M_{max}}$	3.01	4.02
$\tilde{k}_3 = \frac{k_3 [C_s]}{k_2 M_{max}}$	2.15×10^{-2}	1.43×10^{-2}
$\tilde{a}_{12} = \frac{a_{12}}{[c_2]}$	3.1×10^{-2}	1.4×10^{-2}
$\tilde{a}_{22} = \frac{a_{22}}{[c_2]}$	0.12	5.5×10^{-2}
$\tilde{a}_{ps} = \frac{a_{ps}}{[c_1]}$	4.9	6.5
$\tilde{a}_{sb_1} = \frac{a_{sb_1}}{[c_1]}$	0.154	0.205
$\tilde{a}_{01} = \frac{a_{01}}{[c_1]}$	1.5×10^{-2}	2.1×10^{-2}
$\tilde{a}_{02} = \frac{a_{02}}{[c_2]}$	6.2×10^{-3}	2.8×10^{-3}
$\tilde{a}_{ps_1} = \frac{a_{ps_1}}{[c_1]}$	31	41

to consider the corresponding processes as fast compared to the activation of anti-inflammatory macrophages, which sets our reference timescale. As a result, the system only separates into two meaningful timescales.

To reveal the cytokine dynamics on the short timescale, we make use of the small parameters ε_{c_1} and ε_{c_2} and rescale time via $\tilde{t} = \varepsilon_{c_1} \tilde{t}_F$, where $\tilde{t}_F = O(1)$. After substituting this rescaled time into Equations (13)–(19) and keeping only the $O(1)$ terms, we see that the debris and cell populations do not evolve on this timescale (to leading order), and therefore remain at their initial values. The governing equations for the evolution of cytokine concentrations are then:

$$\frac{d\tilde{c}_1}{d\tilde{t}_F} = \frac{\tilde{a}_{12}}{\tilde{a}_{12} + \tilde{c}_2} \tilde{k}_0 - \tilde{c}_1, \quad \frac{\varepsilon_{c_2}}{\varepsilon_{c_1}} \frac{d\tilde{c}_2}{d\tilde{t}_F} = \frac{C_s(0)}{[C_s]} \frac{\tilde{a}_{22}}{\tilde{a}_{22} + \tilde{c}_2} \tilde{k}_3 - \tilde{c}_2 \tag{21}$$

which we solve subject to the initial conditions $\tilde{c}_1 = 1.5$ (male) or $\tilde{c}_1 = 2.05$ (female), and $\tilde{c}_2 = 0$ for both sexes. In this early stage response, we see that the cytokine dynamics are driven by production of pro-inflammatory cytokines in response to debris ($\tilde{k}_0$) and anti-inflammatory cytokines by SSPCs ($\tilde{k}_3$), together with natural cytokine decay.

On the long timescale $\tilde{t} = O(1)$, the small terms of $O(\varepsilon_{c_1})$ and $O(\varepsilon_{c_2})$ in Equations (17) and (18) can be neglected. As a result, the cytokine concentrations reach a quasi-steady state and are determined by solution to the following algebraic equations:

$$0 = \frac{\tilde{a_{12}}}{\tilde{a_{12}} + \tilde{c}_2} \left(\tilde{k}_0 \tilde{D} + \tilde{M}_1 \right) - \tilde{c}_1, \quad 0 = \frac{\tilde{a_{22}}}{\tilde{a_{22}} + \tilde{c}_2} \left(\tilde{M}_2 + \tilde{k_3} \tilde{C}_s \right) - \tilde{c}_2. \tag{22}$$

The dynamics of the debris and the cell populations then evolve according to Equations (13)–(16) and Equation (19), in which the expressions for the cytokine concentrations are obtained from Equations (22). These equations are solved subject to the initial conditions $\tilde{D} = 1$, $\tilde{M}_1 = \tilde{M}_2 = 0$, and $\tilde{C}_s = 1 \times 10^{-2}$ together with $\tilde{M}_0 = 4 \times 10^{-3}$ (male) or $\tilde{M}_0 = 2.7 \times 10^{-3}$ (female).

In Section 3.3, we present the results from the short and long timescale solutions alongside the solution of the full EH submodel corresponding to Equations (13)–(19).

2.5 Implementation details

The ODE model and its reduced formulation were implemented in MATLAB R2024b (The MathWorks Inc., Natick, MA, USA). Simulations were performed using the male and female parameter values specified in Section 2.3. The global sensitivity analysis was implemented in MATLAB, while the corresponding heatmaps were generated in R Statistical Software (v4.4.3; [67]). Simulations were performed using the stiff solver ODE23s, which is suitable for systems with components evolving on different timescales. In the case of the full-dimensional model, a total duration of 400 post-fracture days (PFDs) was simulated to capture the complete bone healing process, including the late phases of bone formation. The scripts used for the simulations and analyses are available in the following GitHub repository: https://github.com/LauraLafuenteG/Sex-differences.

Local sensitivity analyses of the non-zero initial conditions were performed to assess the robustness of model predictions to uncertainty in the initial fracture environment. Details and results are provided in Section S3 of the Supplementary material.

To analyze the numerical results quantitatively, three output metrics were calculated for each model outcome and for both male and female simulations: peak value, time-to-peak, and area under the curve (AUC). The AUC was computed using the MATLAB `trapz()` function over the full 0 to 400 PFD time range. Male-to-female and female-to-male ratios were then calculated for the AUC to facilitate comparisons between the sexes. Complete tables of these metrics are provided in Section S4 of the Supplementary material.

The model was validated for the male and female cases by comparing their numerical results with experimental data on femur osteotomies in young (12-week-old) male and female mice from Haffner-Luntzer et al. [12]. Note that this study was not used to derive the model parameter values, but rather serves as an independent *in vivo* data set for model validation. The outcome of this validation is discussed in Section 3.4.

3 Results

We start by presenting the results of the global sensitivity analysis in Section 3.1. This analysis identifies the biological processes that most influence model predictions and supports the relevance of sex-specific parameters. We then consider the reduced early-healing (EH) submodel in Section 3.2, which illustrates the dominant dynamics on the short and long timescales. The male and female dynamics operate on the same timescales but show quantitative differences between the predictions for the debris and cell densities, as well as the cytokine concentrations. To illustrate these quantitative

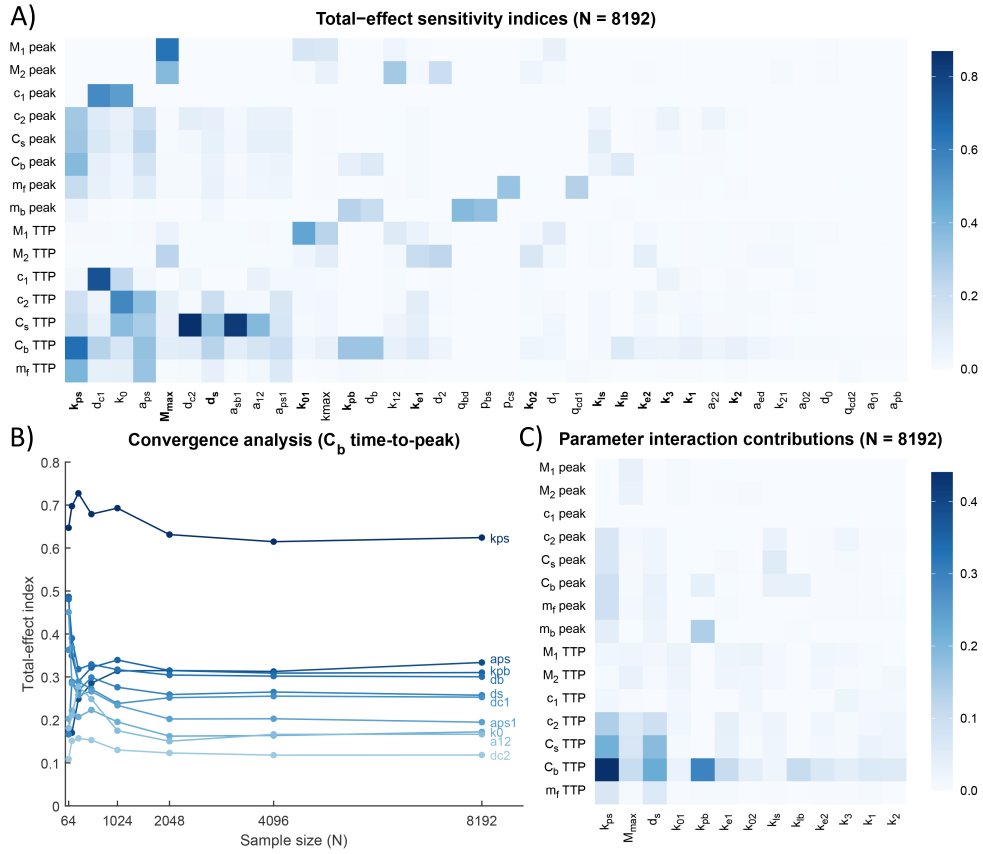


Fig. 3 Variance-based global sensitivity analysis of the baseline parameter set. (A) Heatmap of total-effect sensitivity indices (S_{T_i}) for all 37 model parameters and 15 output metrics. Sex-specific parameters are shown in bold. TTP, time-to-peak. (B) Convergence analysis of osteoblast time-to-peak. (C) Heatmap of interaction contributions ($S_{T_i} - S_i$) for the 13 sex-specific parameters. TTP, time-to-peak.

differences, in Section 3.3 we present the results of the full model, which captures the progression of bone fracture healing from inflammation through repair.

3.1 Sensitivity analysis

The resulting total-effect heatmap revealed distinct sensitivity patterns across the inflammatory and repair phases of healing (Fig. 3A). The main sensitivity patterns are summarized below, while the complete results are presented in Sections 1.2 and 1.3 of the Supplementary material. Convergence of the sensitivity indices across increasing sample sizes supported the selection of $N = 8192$ for the final analysis (Fig. 3B).

Early inflammatory outputs are controlled by direct effects. Macrophage-related outputs (M_1 and M_2) are governed by a small number of parameters with predominantly direct effects. The maximal macrophage density (M_{max}), which in our

model is sex-specific, dominates three of the four related outputs: peak values of M_1 and M_2, and M_2 time-to-peak (Fig. 3A). Three additional parameters in this subset are also sex-specific: the activation rate of M_0 to M_1 (k_{01}), which is the dominant parameter for the time-to-peak of M_1, and the complementary activation rate of M_0 to M_2 (k_{02}) and the debris removal rate by M_1 (k_{e_1}), both of which strongly influence the time-to-peak of M_2. Both output metrics of the pro-inflammatory cytokines (c_1) are governed almost entirely by the direct effects of pro-inflammatory cytokine degradation (dc_1) and production (k_0).

Transition-phase outputs reveal a shift from direct regulation to interaction-driven dynamics. Compared with the other inflammatory outputs, anti-inflammatory cytokines (c_2) exhibit a broader sensitivity profile, being influenced by both inflammatory- and SSPC-related parameters. Interestingly, c_2 and SSPCs (C_s) display a similar balance between direct (Fig. 3A) and interaction effects (Fig. 3C): peak values are mainly dominated by direct effects and time-to-peak metrics by parameter interactions. For both c_2 and C_s, the peak value is dominated by the direct contribution of the sex-specific SSPC proliferation rate (k_{ps}), which also remains one of the dominant parameters for their time-to-peak. Another sex-specific parameter, the SSPC differentiation rate (d_s), is likewise among the most influential contributors to both time-to-peak outputs. For c_2 time-to-peak, the dominant parameter is k_0 (production of pro-inflammatory cytokines), whereas SSPC time-to-peak is primarily governed by interactions involving the anti-inflammatory cytokine decay rate (d_{c_2}) and the effectiveness of c_1 inhibition of SSPC differentiation (a_{sb_1}). In contrast to the earlier inflammatory outputs, the timing of both c_2 and C_s emerges from parameter interactions rather than individual parameter effects, indicating that the transition from inflammation to repair coincides with a shift from direct regulation to increasingly interaction-driven healing dynamics.

Repair outputs are strongly influenced by inflammation–repair coupling. The sensitivity patterns identified for anti-inflammatory cytokines (c_2) and SSPCs (C_s) persist into the repair phase, particularly for osteoblasts (C_b) and, to a lesser extent, fibrocartilage (m_f) (see Fig. 3A). The sex-specific SSPC proliferation rate (k_{ps}) remains one of dominant contributors, controlling osteoblast peak value and time-to-peak, as well as fibrocartilage time-to-peak. The time-to-peak of osteoblasts is largely governed by interaction-driven dynamics involving cytokine and SSPCs processes. Several of the influential parameters are sex-specific, including the osteoblast proliferation rate (k_{pb}), SSPC differentiation rate (d_s), maximal osteoblast density (k_{lb}), and debris removal rate by M_1 (k_{e_1}). The latter also contributes to osteoblast peak value, further illustrating the persisnt influence of inflammatory processes on repair-related outcomes. In contrast, fibrocartilage (m_f) and woven bone (m_b) peak values are mainly governed by their tissue-specific processes.

Sensitivity patterns support the relevance of sex-specific processes throughout healing. Taken together, the sensitivity analysis reveals a clear distinction between peak-value and time-to-peak outputs. Peak values are generally controlled by a limited number of parameters with predominantly direct effects, indicating that the magnitude of biological responses can largely be attributed to individual processes. In contrast, time-to-peak metrics are governed by a broader set

of influential parameters and exhibit stronger interaction effects, particularly as the healing process progresses, indicating that the timing of healing emerges from interactions between inflammatory, SSPC-, and osteoblast-related processes. This distinction is also evident from the interaction-contribution heatmap (Fig. 3C), where interaction contributions are consistently larger for time-to-peak outputs than for peak-value metrics. Furthermore, influential sex-specific parameters are present throughout the healing cascade, regulating the dynamics of macrophages (M_{max}, k_{e_1}, k_{01}, k_{02}), SSPCs (k_{ps}, d_s), and osteoblasts (k_{lb}, k_{pb}). As a result, every stage of healing is controlled by processes that include sex-specific parameters. Thus, the global sensitivity analysis and the literature-based parameterization independently converged on the same biological mechanisms, supporting the relevance of introducing sex-specific parameters and suggesting that sex differences are expected to influence both inflammatory and repair outcomes.

3.2 Early-healing submodel

The reduced EH submodel described in Section 2.4 reveals the underlying timescales of the early fracture healing response, comprising the inflammatory phase and the subsequent pro-regenerative state. Using the dimensionless parameter values of Table 4, the EH submodel reveals two common timescales for both the male and female cases: a short timescale associated with the cytokine response (Fig. 4) and a long timescale associated with the debris and cell dynamics (Fig. 5).

Figure 4 shows the dimensionless cytokine concentrations for the male (blue lines) and female (red lines) parameter sets. Note that the corresponding dimensional scales differ between the male and female cases (see Table 3). In all cases, the full EH submodel solution of Equations (13)–(19) is given by solid lines, the short-timescale solution by dashed-dot lines, and the long-timescale solution by dashed lines. Since the EH submodel only captures processes up to C_s, the long timescale is relative and reflects the slower behavior of the early healing response. The insets highlight the close agreement between the full EH solution and the short-timescale solution at early times. The short-timescale solution captures the rapid transition of the cytokine concentrations from their initial values to the corresponding concentrations at which cytokine production and decay balance. These values, obtained from the steady-state solutions of Equations (21), are indicated by dotted horizontal lines in the insets. During this period of rapid cytokine adjustment, the cell populations remain well approximated by their initial values. The dashed lines indicate the quasi-steady state solutions for cytokine concentrations, which depend on debris and cell density dynamics, as determined by the solution to Equations (22) together with Equations (13)–(16) and Equation (19). As seen in Fig 4, this long-timescale prediction is accurate for longer times but, as expected, is less accurate for very early times. Note that the error between the long-timescale prediction and the full EH solution for early times is at most approximately 10%. The long-timescale reduced model neglects terms that are small in the parameters ε_{c_1} and ε_{c_2}, and we therefore anticipate errors when comparing the predictions of the long-timescale submodel and the full EH model. The approximately 10% error observed is consistent with the size of these small parameters.

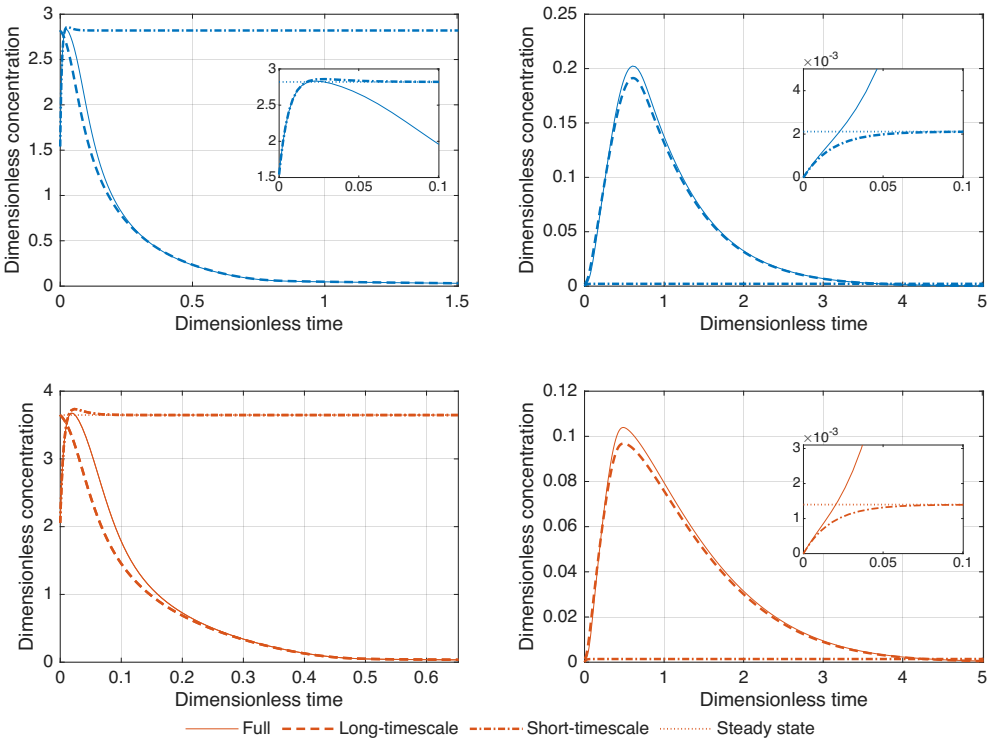


Fig. 4 Predicted cytokine concentrations for the male (top row, blue) and female (bottom row, red) cases. Left: pro-inflammatory cytokine concentration ($\tilde{c}_1$). Right: anti-inflammatory cytokine concentration ($\tilde{c}_2$). Solid line: full solution; dashed line: long-timescale solution; dashed-dot line: short-timescale solution. Insets show close up comparison of full EH (solid line) and short-time (dashed-dot) solutions at early times, together with the steady state solutions of Equations (21) (dotted line). Note that the x- and y-axes are different. All results are plotted against dimensionless male time to facilitate direct comparison of the dynamic response of the male and female cohorts.

Figure 5 shows the predictions of the long-timescale reduced model for the debris and cell densities (dashed lines) compared with the predictions obtained by solving the full EH submodel of Equations (13)–(19). Blue and red lines denote male and female cases, respectively. For visualization purposes, all results are plotted against dimensionless male time to facilitate direct comparison of the dynamics between the two cohorts; that is, the dimensionless time is normalized with respect to the male value of k_{02}. We see that, in general, the agreement between the reduced and the full EH submodel predictions is excellent. The largest discrepancies occur in the SSPC predictions for the SSPCs, reflecting the impact of cytokine concentrations on the rates of SSPC production and decay (see Equation (19)), whereas cytokines have much less impact elsewhere in Equations (13)–(16). As a result, any discrepancy in the cytokine predictions between the long-timescale and the full EH submodel solutions directly affects the predicted SSPC dynamics, as seen in Fig. 5 (left). Nevertheless,

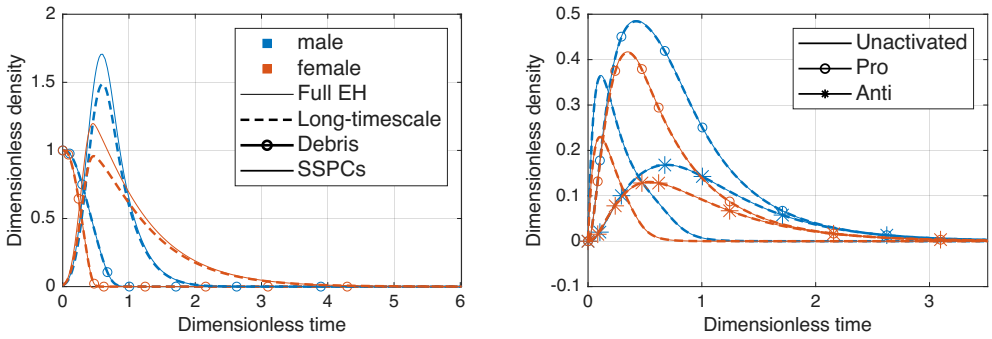


Fig. 5 Predicted debris and cell densities for the male (blue lines) and female (red lines) cases. Left: debris ($\tilde{D}$) and skeletal stem/progenitor cells ($\tilde{C}_s$). Right: unactivated ($\tilde{M}_0$), pro- ($\tilde{M}_1$) and anti-inflammatory ($\tilde{M}_2$) macrophages. Solid line: full solution; dashed line: long-timescale solution. Note that the x- and y-axes are different. All results are plotted against dimensionless male time to facilitate direct comparison of the dynamic response of the male and female cohorts.

this disagreement is small and within the error anticipated given the size of the ε parameters.

While these results indicate that the timescales of the male and female dynamics are the same, there are quantitative differences in the predictions on each timescale. As the results have been presented in dimensionless form, there will also be quantitative differences in the dimensional predictions for the debris and cell population densities and the cytokine concentrations, reflecting the different dimensional quantities for the male and female cases. To interrogate these differences in more detail and present dimensional predictions that align with experimental measurements, as well as further scrutinize sex differences in the repair phase in terms of osteoblast, fibrocartilage, and bone density, in the next section we present a detailed examination of the full dimensional model capturing the healing process from inflammation through repair.

3.3 Full model

The model described in Section 2.1 predicts the temporal evolution of the inflammatory and repair phases of the bone fracture healing process in males and females. Using the parameter values of Tables 2 and 3, the model predicts a successful healing outcome for both males and females, which is defined by the complete down-regulation of the inflammatory response (Fig. 6) and the full ossification of the callus (Fig. 7).

At post-fracture day (PFD) 0, the presence of non-activated, tissue-resident macrophages and skeletal stem/progenitor cells (SSPCs), the accumulation of debris resulting from the fracture event, and the immediate release of pro-inflammatory cytokines triggered by macrophage recognition of debris are represented by the non-zero initial conditions of M_0 (Fig. 6D), C_s (Fig. 7A), D (Fig. 6A), and c_1 (Fig. 6B), respectively, reflecting the background state of the system at the onset of healing (see Equations 11). In response to debris accumulation, macrophages are further recruited within the first 24 hours (Fig. 6D), and additional pro-inflammatory cytokines are rapidly secreted (Fig. 6B). Macrophages activate faster in females (parameters k_{01} and

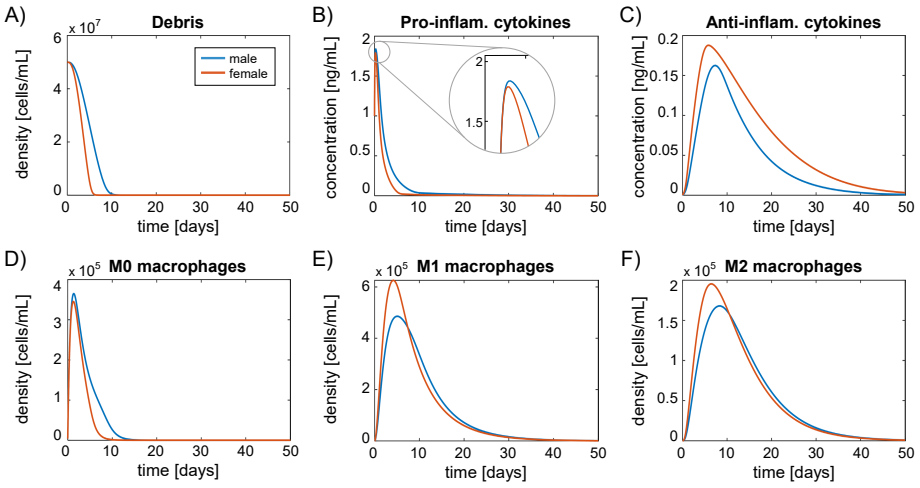


Fig. 6 Predicted inflammatory response for the male (blue lines) and female (red lines) cases. The plots represent the temporal evolution of the average (A) debris density (D); (B) pro- (c_1) and (C) anti-inflammatory (c_2) cytokines concentration; and (D) unactivated (M_0), (E) pro-inflammatory (M_1), and (F) anti-inflammatory (M_2) macrophage density. Note that the y-axes are different.

k_{02} in Table 3), leading to a slightly lower peak of unactivated macrophages (Fig. 6D). For males, the complete activation of macrophages takes longer: macrophage polarization in males is completed by PFD 15, in contrast with PFD 10 in females (see Fig. 6D). Once the macrophages polarize into either M1 or M2, they remove the debris by phagocytosis. In our model, females are assigned a higher maximal macrophage density (parameter M_{max} in Table 3), allowing for a larger macrophage population. While the model predicts higher peaks of both M1 (Fig. 6E) and M2 (Fig. 6F) macrophages in females, the total macrophage population, measured as the sum of the areas under the curves (AUCs) of the variables M_0, M_1, and M_2, is nearly the same between the sexes, with a female-to-male ratio of 0.99. Both M1 and M2 peaks occur earlier in females, at PFD 4 and 6, in comparison to males, at PFD 5 and 8. Female macrophages also have enhanced phagocytic capacity (parameters k_{e_1} and k_{e_2} in Table 3); hence, debris is cleared in a shorter time for females (Fig. 6A), i.e. by PFD 6 as compared to PFD 11 in males.

In our model, female macrophages are parameterized to secrete fewer pro-inflammatory and more anti-inflammatory cytokines (parameters k_1 and k_2 in Table 3). Additionally, female SSPCs are parameterized with a higher immunosuppressive capacity (parameter k_3 in Table 3), which further enhances the production of anti-inflammatory cytokines. This trend is observed in the predicted results shown in Fig. 6B-C: male cells produce higher levels of pro-inflammatory cytokines (Fig. 6B), while female cells secrete greater amounts of anti-inflammatory cytokines (Fig. 6C). Although the qualitative difference in pro-inflammatory cytokine production seems relatively small, the AUC of c_1 reveals a male-to-female ratio of 1.63, indicating that male macrophages secrete significantly higher levels overall. In contrast, the AUC

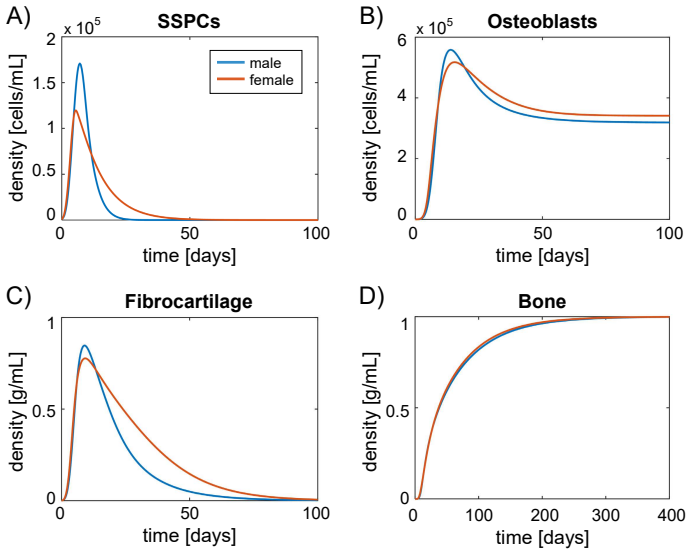


Fig. 7 Predicted repair response for the male (blue line) and female (red line) cases. The plots represent the temporal evolution of the average density of (A) SSPCs (C_s), (B) osteoblasts (C_b), (C) fibrocartilage (m_f) or soft callus, and (D) woven bone (m_b) or hard callus. Note that the x- and y-axes are different per panel.

of c_2 shows a female-to-male ratio of 1.52, confirming that females produce more anti-inflammatory cytokines, as observed qualitatively. For both cytokine types, the peak production occurs earlier in females than in males. Pro-inflammatory cytokines peak within the first 24 hours for both sexes and exhibit a rapid burst within the first 10 PFDs (Fig. 6B), reflecting the acute inflammatory response. Conversely, anti-inflammatory cytokines peak before PFD 6 for females and at PFD 7 for males, maintaining a sustained production for over 50 PFDs in females and around 40 PFDs in males (Fig. 6C).

Consequently, since inflammation is considered active when any of the variables M_1, M_2, c_1, or c_2 are positive (see Section 2.1), the predicted inflammatory response is stronger and persists slightly longer in the female model. This is mainly driven by higher peaks of M1 and M2 macrophages in females, although both sexes show similar decay patterns afterward (Fig.6E-F), and by consistently higher secretion of anti-inflammatory cytokines in females, both during the peak and throughout the decay phase.

As discussed in Section 1.1, the inflammatory and repair phases are interdependent. Tissue-resident SSPCs are represented by the non-zero initial condition of SSPCs, and their numbers increase due to recruitment by pro-inflammatory cytokines. In the model, this recruitment is incorporated into the SSPC proliferation term (A_s in Equation 7). Female SSPCs are assigned a lower maximal density (parameter k_{ls} in Table 3), limiting the maximum size of the SSPC population. This, along with reduced pro-inflammatory cytokine secretion, results in a significantly lower peak of SSPCs in

females compared to males (30% less, see Fig. 7A). The SSPC peak occurs at PFD 5 in females and at PFD 7 in males, just hours before the peak of anti-inflammatory cytokines on the same PFDs. This timing is consistent with the role of SSPCs as immunosuppressors, which increase the production of anti-inflammatory cytokines (see Equation 6). Despite the lower peak of SSPCs in females, the proliferation rate of female SSPCs is higher in our model (parameter k_{ps} in Table 3). As a result, the cumulative number of SSPCs over the course of healing, as measured by the AUC, is very similar between the sexes, with a female-to-male ratio of 1.14.

In our model, the fibrocartilage or soft callus is produced solely by the SSPC population, so the fibrocartilage dynamics reflect the trend predicted for these early repair cells. Despite the fibrocartilage peak occurring at PFD 9 in both the male and female cases, the higher number of male SSPCs leads to a higher peak in males (Fig. 7C). Conversely, the slower differentiation rate in our female model (parameter d_s in Table 3) allows SSPCs more time to proliferate, resulting in a soft callus that persists significantly longer. While the peak in the male model diminishes by half at PFD 20, the peak in the female model only reaches half of its maximum at PFD 30 (Fig. 7C). Consequently, the overall fibrocartilage density, measured by the AUC, is higher for females, with a female-to-male ratio of 1.39.

Similarly to SSPC behavior, female osteoblasts in our model are parameterized with a lower maximal density and a higher proliferation rate (parameters k_{lb} and k_{pb} in Table 3). Together with the weaker osteogenic differentiation from female SSPCs, these sex-specific parameters lead to the following results. The osteoblast peak occurs earlier in males (by PFD 14) compared to females (at PFD 15) and reaches a higher value, although the difference is less pronounced than in the SSPC peak (7% vs. 30%; Fig. 7B). As observed for SSPCs, the higher proliferation rate of female osteoblasts compensates for their initially lower cell numbers. As a result, the female model predicts slightly higher osteoblast numbers once the population stabilizes, although the difference compared to males is small. When considering the osteoblast density throughout the healing process, measured by the AUC, the female-to-male ratio is 1.07, indicating that males and females exhibit similar cumulative osteoblast numbers.

In our model, woven bone or hard callus is produced exclusively by osteoblasts. Consequently, the osteoblast dynamics are further reflected in the woven bone trend (Fig. 7D), which shows a very similar ossification pattern in both sexes, both qualitatively and quantitatively. The bone relative area reaches 99% by PFD 286 in both males and females, and the overall hard callus density, measured by the AUC, yields a female-to-male ratio of 1.01. Finally, regarding the general healing timeline, both male and female cases predict that osteoblast numbers stabilize within weeks, indicating a positive healing trajectory, while full ossification takes several months to complete.

3.4 Validation with independent *in vivo* data

In the *in vivo* experiments reported by Haffner-Luntzer et al. [12], female and male mice underwent femur osteotomy at 12 weeks of age. Mice were sacrificed either 10 days or 21 days after surgery. The relative percentages of fibrous tissue, cartilage, and bone areas within the whole fracture callus were histologically determined. These values are represented by the bars in Fig. 8. At day 10, male mice showed significantly

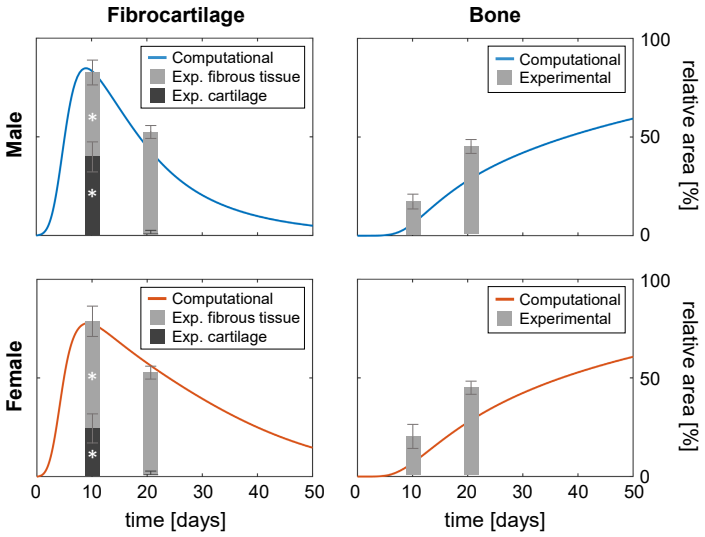


Fig. 8 Computational and experimental evolution of normal fracture healing. Temporal evolution (PFDs) of fibrocartilage and bone tissue fraction (%) as predicted by the model for the male and the female cases (lines), and relative (%) fibrous tissue, cartilage, and bone area as experimentally measured by Haffner-Luntzer et al. [12] (bars, average value ± standard error). The bars represent the quantification at PFD 10 and PFD 21. The fibrous tissue and cartilage bars are stacked. The stars indicate significant sex differences.

more cartilage but less fibrous tissue in the fracture callus compared to female mice, with no significant difference in bone quantity or callus size. This indicates that male mice experience faster cartilaginous callus development [12]. By day 21, the fracture callus in male mice was significantly larger compared to female mice [12], while the relative fibrous tissue, cartilage, and bone areas did not differ. However, male mice exhibited significantly higher tissue mineral density, indicating more mature bone in the fracture callus and a slightly more rapid fracture healing process [12]. Additionally, on both day 10 and day 21, no significant differences in osteoblast numbers between male and female mice were observed [12].

In our computational model, fibrous tissue and cartilage are combined into fibrocartilage, allowing us to predict an equivalent relative tissue area that corresponds to the sum of cartilage and fibrous tissue fractions observed in experimental studies. The predicted fibrocartilage fraction (Fig. 8, left) is 82% for males and 77% for females at PFD 10, and 40% for males and 54% for females at PFD 21. In the experiments by Haffner-Luntzer et al. [12], the combined relative areas of fibrous tissue and cartilage are 83% for males (43% fibrous tissue and 40% cartilage) and 79% for females (55% fibrous tissue and 24% cartilage) at PFD 10, and 52% for both males (52% fibrous tissue and 0.45% cartilage) and females (52% fibrous tissue and 0.15% cartilage) at PFD 21 (values estimated from figures in [12]). Consequently, our predicted fibrocartilage fraction aligns well with the experimentally quantified values at PFD 10 for both males (82% vs. 83%) and females (77% vs. 79%), preserving the trend of accelerated cartilaginous or soft callus formation in males. However, some mismatch is observed

at PFD 21. Quantitatively, the computational value for females agrees with the experimental one (54% vs. 52%); but the predicted value for males is much lower than the experimental quantification (40% vs. 52%).

Regarding bone tissue (Fig. 8, right), our model predicts a relative fraction of 7% for males and 8% for females at PFD 10, and 30% for both males and females at PFD 21. The relative bone areas reported by Haffner-Luntzer et al. [12] are 17% for males and 20% for females at PFD 10, and 45% for both sexes at PFD 21 (values estimated from figures in [12]). This comparison shows a good qualitative agreement between the predicted hard callus formation and the experimental observations for both males and females, as the same ossification pattern is observed. Indeed, at PFD 10 there is slightly more bone formation for females in both the computational and experimental data, whereas the same relative bone area is observed for both sexes at PFD 21. Quantitatively, however, the computational and experimental values do not match: the simulated bone tissue fraction aligns with the experimental data at approximately double the time. That is, *in vivo* observations at PFD 10 and 21 are captured by our models only around PFD 20 and 40, respectively. This discrepancy may result from multiple factors, including the hybrid cross-species parameterization adopted in this study and structural simplifications of the computational model. These limitations are further discussed in Section 4.3.

Finally, the osteoblast dynamics shown in Fig. 7B and discussed in Section 3.3 align with the *in vivo* findings of [12], which reported no significant sex-based differences in osteoblast numbers. Although the simulated osteoblast peak in males is slightly higher and occurs one day earlier, the model predicts similar cumulative osteoblast numbers between sexes when measured by the area under the curve (AUC) throughout the healing process, indicating no substantial sex differences.

In summary, despite some discrepancies, the model predicts realistic healing patterns that align with the experimentally observed behavior for both male and female cases.

4 Discussion

This study aimed to investigate sex differences in normal fracture healing using computational modeling. We focused the analysis on normal healing conditions as a necessary first step toward understanding how sex differences modulate fracture repair dynamics, prior to considering pathological scenarios in future studies. To this end, we revisited the macrophage-mediated model of Trejo et al. [57]. We introduced sex-specific parameter sets derived from available literature on sex differences in bone fracture healing and, in parallel, performed a global sensitivity analysis to identify the biological processes and parameters that contribute most strongly to model predictions. While these analyses were performed independently, they highlighted common biological mechanisms: several parameters identified as sex-specific were also among the most influential parameters governing model outputs. This agreement supports the relevance of incorporating sex-specific processes into computational models of fracture healing and suggests that sex differences can influence both inflammatory and repair responses.

4.1 Timescales as a framework for sex-specific fracture healing dynamics

To explore whether sex differences affect the timing of key biological processes during early fracture healing, a phase shown to be critical for successful bone repair [3], we first performed a timescale analysis of the early-healing (EH) submodel focusing on the inflammatory phase and the subsequent pro-regenerative transition. This was followed by numerical simulations of the full model, which includes both inflammatory and repair responses, to investigate sex-specific dynamics across the entire course of fracture healing.

The timescale analysis of the EH submodel described in Section 3.2 provided insights into the temporal organization of early fracture healing. For both male and female parameter sets, the non-dimensionalized EH submodel revealed two characteristic timescales: a short timescale, on the order of hours, and a long timescale, on the order of days. On the short timescale, pro- and anti-inflammatory cytokine concentrations rapidly adjusted from their initial values to quasi-steady levels, while debris and cell densities remained close to their initial conditions. In contrast, the long timescale governed the evolution of debris, macrophages (unactivated, pro-, and anti-inflammatory), and skeletal stem/ progenitor cells (SSPCs) densities, with cytokine concentrations slave to these dynamics. As the EH submodel focuses on early healing, the long timescale is relative and captures the slower behavior of the inflammatory and pro-regenerative cell populations, excluding later healing stages such as callus formation by repair cells. The comparison between the reduced timescale solutions and the full EH submodel predictions resulted in excellent agreement, confirming that the reduced models accurately capture the relevant dynamics of the EH submodel on their respective timescales.

Although the EH submodel did not reveal sex-dependent timescales, it plays a key interpretative role by establishing a common temporal framework for early fracture healing. Within this framework, sex differences emerge as quantitative shifts rather than as distinct temporal organization of the underlying biological processes. As presented in Section 3.3, the full model predicted sex-specific differences across both the inflammatory and repair phases of fracture healing. Female macrophages activated more quickly and exhibited enhanced phagocytic activity, leading to faster debris clearance and earlier peaks of both pro- and anti-inflammatory cytokines; although pro-inflammatory cytokines peaked within the first 24 hours for both sexes. Females also showed higher macrophage peaks and sustained anti-inflammatory cytokine production, resulting in a stronger and more prolonged inflammatory response. In contrast, males exhibited higher overall levels of pro-inflammatory cytokines but a shorter duration of inflammation. In the repair phase, males reached higher peaks of SSPCs, osteoblasts, and fibrocartilage, while females displayed slower osteogenic differentiation but higher proliferation rates, resulting in more prolonged activity of repair cell populations and leading to similar cumulative numbers of repair cells between the sexes over the course of healing. Consequently, despite differences in the predicted healing trajectories, including both the magnitude and timing of several biological

processes, both sexes achieved similar bone formation dynamics, suggesting that differences along the healing process can still lead to comparable healing outcomes in normal fracture repair.

4.2 Agreement with experimental findings

The sex-specific model predictions are consistent with the experimental findings reported in Section 1.2. Regarding cytokine dynamics, the model reproduces the rapid early inflammatory response and the sex-specific balance between pro- and anti-inflammatory cytokines observed in experimental studies. Peak production occurs earlier in females than in males for both cytokine types; however, these differences remain within the same short cytokine response window. As predicted by the full model, males show greater pro-inflammatory cytokine production and females exhibit higher anti-inflammatory cytokine levels, consistent with the literature data used to inform model reparameterization [8, 14, 15, 28, 30, 31, 34, 35]. As a result, a stronger and more sustained inflammatory response is predicted in females, in agreement with experimental observations of enhanced and prolonged immune responses in females [30, 31].

The dynamics of immune and pro-regenerative cells populations also align well with experimental observations. Regarding immune cell populations, the predicted female macrophages exhibited increased numbers [15, 31, 32] (here shown at the peaks), faster activation rates [30, 31, 33], and enhanced phagocytic activity [15, 30, 32]. Since these experimental results were used to inform model parameters (see Section 2.3), the observed agreements indicate that the model reproduces the expected sex-specific differences. Although debris clearance and macrophage activation and polarization occurred earlier in females, these timing differences represent quantitative shifts within the same long cellular timescale governing macrophage-mediated processes in both sexes. In agreement with experimental studies, anti-inflammatory (M2) macrophages remain active for longer periods than the pro-inflammatory (M1) phenotype [22, 23, 25], a behavior that is captured in the present model as extended dynamics within the long cellular timescale rather than as a distinct additional timescale. In the pro-regenerative transition toward the repair phase, the full model predicted higher peak densities of SSPCs in males, in agreement with experimental reports of increased activated SSPCs in the bone marrow of male rodents [13, 15, 37, 38, 40], which informed model parameters.

The model results were validated against independent *in vivo* data from Haffner-Luntzer et al. [12], who reported no significant sex-based differences in osteoblast numbers and similar ossification patterns between male and female mice, with faster soft callus formation in males [12]. While faster bone formation has been observed in male mice [10, 12, 29], this was quantified by more mature bone within the fracture callus rather than by a greater relative bone area [12]. Accordingly, as discussed in Section 3.4, the full-model predictions are in very close agreement with these *in vivo* findings, including comparable osteoblast numbers between sexes despite a slightly earlier and higher peak in males, accelerated soft callus formation in males, and similar ossification trends between the sexes. Finally, regarding the overall healing timeline,

both male and female simulations predict positive healing trajectories, with full ossification taking several months to complete, consistent with experimental and clinical observations [17, 23].

Additionally, when comparing model results with experimental data, it is important to carefully consider how cell population dynamics are quantified. As discussed, the model predicts higher peak values of both M1 and M2 macrophages in the female case, consistent with experimentally observed increased macrophage numbers in females [15, 31, 32], as well as higher SSPC peak values in the male case, in alignment with experimental findings indicating higher numbers of activated SSPCs in males [13, 15, 37, 38, 40]. However, when cell populations are quantified using cumulative measures such as the area under the curve (AUC), the full model predicts similar cumulative numbers of M1 and M2 macrophages between the sexes, while cumulative SSPC numbers are higher in females than in males. This apparent difference between peak and cumulative values does not necessarily indicate a contradiction, but rather reflects different aspects of the same underlying dynamics. Experimental studies often report cell counts at a limited number of discrete time points, whereas in the model the AUC captures cumulative cell numbers over the entire healing process. This distinction is particularly relevant for macrophages and SSPCs, which act primarily during an early and relatively brief phase of healing, making cumulative measures sensitive to shifts in timing. This is not the case, for example, for osteoblasts, whose prolonged activity during the ossification process makes their cumulative numbers less dependent on precise timing.

Despite the strong overall alignment between model predictions and experimental observations, some biological processes in the model occur more slowly than reported in the literature. For example, the acute inflammatory response in humans typically resolves within 7 post-fracture days (PFDs) [23]. In contrast, high numbers of M1 macrophages, which characterize the acute inflammatory response, persist beyond this 7-PFD period in the model. While experimental data report that macrophages remain present throughout the entire healing process [3, 17, 25], their dominant phenotypes evolve over time. As result of injury, inflammatory macrophages are recruited and initially polarize into the M1 phenotype, which dominates the early stages of healing, and later shift to the M2 phenotype, which promotes tissue repair. Therefore, while the presence of M2 macrophages is expected beyond the resolution of the acute inflammatory response, the prolonged presence of M1 macrophages can be detrimental to bone healing [17, 25]. Nonetheless, both numerical and timescale results capture the qualitative pattern of macrophage dynamics, with M1 macrophages declining earlier than M2 macrophages.

One possible explanation for the slower resolution of inflammation lies in the relative separation of timescales in the model. Under the current parameter values, the timescale analysis of the EH submodel identified two dominant timescales: a fast, cytokine-dominated response and a slower, cellular-dominated response. Although the densities of debris, unactivated macrophages, M1 macrophages, and SSPC all evolve more slowly than cytokine concentrations, their separation from M2 macrophage dynamics is not sufficiently strong to generate an additional intermediate timescale. As a result, both M1 and M2 macrophage populations evolve on the same broad cellular

timescale in the model. However, if the kinetic rates governing the dynamics of debris, unactivated and M1 macrophages, and SSPCs were reduced by an order of magnitude, the system would instead exhibit three disparate timescales, with M2 macrophages acting on the slowest one. Such behavior would be consistent with experimental observations indicating that M2 macrophages remain active longer than M1 macrophages [22, 23, 25], as M2 macrophages resolve inflammation and initiate regeneration. This dependence on parameter values highlights the sensitivity of the identified timescale structure and suggests that future work should focus on more rigorous, potentially sex-specific quantification of cellular kinetics to determine whether two or three distinct timescales are at play.

In summary, while some quantitative discrepancies exist in the timing of cellular processes, the model robustly reproduces key qualitative patterns and sex-specific trends observed in experimental studies. These consistencies underscore the relevance of the modeling approach for investigating sex differences in fracture healing. Beyond describing observed biological patterns, the combined use of timescale analysis and full-model simulations offers substantial interpretative power, enhancing our understanding of the biological processes driving these sex-specific differences. As shown in this study, timescale analysis first identified two dominant timescales within the early healing phase, thereby defining a shared temporal framework for the underlying biological processes. Within this framework, full-model simulations revealed biologically relevant sex-specific differences in inflammatory, pro-regenerative, and repair responses and captured their coupled evolution across the entire healing process. Together, these approaches enable a qualitative interpretation of early-phase dynamics and a quantitative assessment of long-term healing trajectories, supporting a comprehensive view of sex-specific fracture healing from the onset of inflammation through hard callus formation and demonstrating the strength of combining complementary computational methods in biomedical modeling.

4.3 Toward a fully experimentally informed model

To explore sex-specific bone fracture healing, we adapted the ordinary differential equation (ODE) system of Trejo et al. [57] by incorporating sex-specific parameter values. As a consequence of the ODE-based formulation, sex differences were captured only in the temporal dynamics. As a result, our sex-specific model lacks spatial resolution, which is critical for incorporating anatomical and biomechanical differences between sexes. For example, preclinical studies on rodents report that males typically exhibit larger callus sizes than females [8, 10, 12, 13, 40], likely due to differences in body weight. Additionally, Allen et al. [28] observed sex-specific differences in cell migration and proliferation, suggesting that spatial aspects of the healing process may differ between sexes.

Furthermore, due to modeling assumptions, the current model by [57] includes only two types of repair cells: skeletal stem/progenitor cells (SSPCs), which in the model produce fibrocartilage, and osteoblasts, which form bone. When creating the sex-specific models informed and validated by the literature data presented in Section 1.2, this creates two additional limitations.

First, there is no distinction between fibrous tissue and cartilage, preventing direct comparison with histological findings and sex-specific differences in their formation. For instance, our model predicts accelerated fibrocartilage formation in males, as indicated by a higher peak reached at the same time as in females, and higher cumulative fibrocartilage density in females, as measured by the area under the curve (AUC). While the higher fibrocartilage peak in males aligns with the combined data on early fibrous tissue and cartilage formation reported by Haffner-Luntzer et al. [12], the biological interpretation of the higher cumulative fibrocartilage density in females is less clear. Since the model does not distinguish between fibrous tissue and cartilage, it is uncertain whether this elevated density reflects increased fibrous tissue, increased cartilage, or a combination of both. If it primarily reflects fibrous tissue, this would be consistent with *in vivo* data showing more fibrous tissue in the fracture callus of female mice [12]. Conversely, if it instead reflects greater cartilage production, it would contradict experimental findings reporting reduced cartilage formation in females, both *in vivo* [12] and in human SSPC-derived organoids [42]. Consequently, the current lumped representation prevents the assessment of potentially distinct sex-specific effects on fibrous tissue and cartilage formation.

Second, the model lacks the endochondral ossification pathway; that is, it does not include the differentiation of SSPCs into chondrocytes and the subsequent cartilage mineralization. Instead, it captures only direct osteogenic differentiation from SSPCs to osteoblasts. While both ossification pathways are involved in bone fracture healing (see Section 1.1), simplifying the model to include only direct osteogenic differentiation limits the ability to interpret sex-specific *in vivo* data related to ossification. In particular, several studies report that male mice exhibit faster bone formation due to accelerated endochondral ossification [10, 12, 29], resulting in more mature bone within the fracture callus than in female mice at the same time point, and thereby indicating a faster healing process [12]. In contrast, while the sex-specific model predicts distinct soft callus dynamics, the predicted bone formation trajectory is very similar for both sexes. This similarity may reflect the simplified representation of ossification in the model, which does not capture sex differences arising from cartilage mineralization and endochondral bone formation. This modeling assumption may also contribute to the quantitative differences between model predictions and experimental observations discussed in Section 3.4. Alternatively, these observed differences may result from the hybrid cross-species parameterization adopted in this study. As both explanations remain plausible, the relative contributions of model structure and parameterization cannot be determined from the present results.

Given that many existing fracture healing models capture spatiotemporal dynamics as well as more detailed cellular lineages and ossification pathways (see [21, 49–55] for extensive reviews), these three modeling limitations will be addressed in future studies.

In addition to modeling constraints, another set of limitations concerns the biological scope of the study and the availability of sex-specific data. Our objective was to demonstrate that sex differences influence bone fracture healing. To achieve this, we developed male and female proof-of-concept models by modifying parameters for which sex-specific evidence was available. However, as explained in Section 2.3, the current state-of-the-art does not provide sufficient data to inform all model parameters:

for some, the available evidence was conflicting or unclear; for others, no sex-specific data were found at all. Where data were lacking or inconsistent, we prioritized human findings when possible and otherwise retained baseline values. For cytokines, sex-specific evidence was interpreted at the level of aggregate pro-inflammatory and anti-inflammatory responses represented in the model, rather than at the level of individual cytokines. The limited availability of sex-specific data led to the hybrid calibration strategy adopted in this study, in which evidence from multiple experimental sources was combined because no single species currently provides comprehensive sex-specific evidence across all stages of bone healing.

Future work should focus on filling these data gaps to explore the sex-specific nature of all parameters and, consequently, of all modeled biological processes. Furthermore, while our model validation focused on repair phase outcomes using available sex-specific fibrous tissue, cartilage, and bone data, it would be valuable to obtain data on the inflammatory response for both sexes, such as macrophage dynamics and cytokine profiles at different time points, to validate the model predictions and timescale separation during the early phase of bone healing, where sex differences may be particularly relevant. Beyond improving parameterization, such larger sex-specific datasets would also enable uncertainty quantification based on parameter distributions, allowing uncertainty to be propagated through the model and the confidence of predicted fracture-healing trajectories to be assessed. Moreover, more comprehensive human sex-specific datasets would reduce reliance on cross-species evidence and facilitate the development of more clinically relevant computational models for the design and evaluation of patient-specific therapeutic strategies.

Due to the complexity of exploring sex differences, we focused on young males and females of reproductive age. Consequently, age is a critical factor not addressed in this study, although previous computational models have successfully incorporated aging [68–70]. While females in their reproductive years typically exhibit enhanced immune responses following injury, this advantage is lost with aging [71]. Advanced age is also associated with dysregulated inflammatory and repair responses in both male and female mice, which compromise fracture healing [8]. These observations underscore the importance of extending future models beyond young populations to capture age-dependent variations in healing outcomes.

Furthermore, within the young female population, we did not account for physiological states such as the menstrual cycle, pregnancy, or lactation, as only preliminary literature is available on these topics [27, 32, 71, 72]. These factors are known to influence bone biology and may affect fracture healing. For example, bone turnover [27] and immunity [32] fluctuate during the menstrual cycle, while pregnancy has been associated with accelerated fracture healing but also induces bone loss due to increased calcium demands [27, 72]. As more data become available, future models should incorporate these physiological states to better reflect intra-sex variability.

Lastly, while this study focuses on normal fracture healing, compromised healing outcomes such as delayed- and non-healing are highly relevant clinically and affect both sexes across all ages. These pathological scenarios involve biological mechanisms such as unresolved inflammation or impaired angiogenesis, which are likely to interact with sex-specific factors. As our understanding of sex-specific dynamics in normal healing

deepens and experimental data continue to expand, future studies should aim to incorporate these more complex scenarios. This will not only broaden the biological scope of the model but also contribute to the development of a fully experimentally informed framework for patient-specific computational modeling of bone fracture healing.

5 Perspectives and significance

To our knowledge, this study is the first to incorporate sex-specific responses into a computational model of bone fracture healing. Given that most preclinical research has traditionally focused on male subjects [11, 73–75], except for research on pathologies that primarily affect females, such as multiple sclerosis or osteoporosis, where the opposite bias exists [75], the development of sex-specific computational models represents an important step toward more inclusive and personalized approaches to bone repair. Such models provide a reproducible, low-cost methodology for hypothesis testing, enabling deeper understanding into the biological mechanisms that underlie fracture healing and how they differ between sexes. As a result, computational models such as the one presented here can play a key role in complementing experimental studies and supporting the design and optimization of patient-specific therapies. Overall, this work lays the groundwork for integrating sex-specific biology into computational modeling and contributes to advancing personalized approaches in musculoskeletal research.

6 Conclusion

This study presents a sex-specific computational model for investigating bone fracture healing dynamics. By revisiting an existing model of the inflammatory and repair phases and incorporating literature-derived sex-specific parameter values, the resulting model integrates diverse experimental data into a unified framework. Global sensitivity analysis independently identified several of these parameters among the most influential drivers of model dynamics, providing additional support for the incorporated sex-specific mechanisms. Within this framework, mechanistic differences between females and males emerge across inflammatory and repair responses, leading to distinct healing trajectories that nevertheless converge toward comparable healing outcomes. The agreement between model predictions and independent experimental observations further supports the biological relevance of the approach. By enabling the interpretation of fracture healing processes in a sex-specific context, this work highlights the importance of incorporating sex as a biological variable in computational modeling and provides a foundation for future extensions toward more detailed and personalized approaches in musculoskeletal research.

List of abbreviations

AUC: area under the curve
BMP: bone morphogenetic protein
EH submodel: early-healing submodel

FGF: fibroblast growth factor
IL: interleukin, e.g. IL-1: interleukin 1
M1 macrophages: pro-inflammatory macrophages
M2 macrophages: anti-inflammatory macrophages
ODE: ordinary differential equation
OPG: osteoprotegerin
PFD: post-fracture day
RANKL: receptor activator of nuclear factor kappa-B ligand
SSPCs: skeletal stem/progenitor cells
TNF-α: tumor necrosis factor alpha
TTP: time-to-peak

Declarations

Ethics approval and consent to participate

Not applicable.

Consent for publication

Not applicable.

Availability of data and materials

The computational codes generated in this study are available in the following GitHub repository: https://github.com/LauraLafuenteG/Sex-differences.

Competing interests

The authors declare that they have no competing interests.

Funding

LL and LG were supported by the European Union's Horizon 2020 program (JOINT-PROMISE, grant number 874837), the European Research Council (ERC; INSTant CARMa, grant number 101088919), the Research Foundation Flanders (FWO Vlaanderen; mERCATOR, grant number G0D0623N), and the Regenerative Medicine Crossing Borders initiative (www.regmedxb.com) powered by the Flemish Government. PA was supported by the Research Foundation Flanders (FWO Vlaanderen, grant number 1S87725N). AC was supported by the Gravitation Program "Materials Driven Regeneration", funded by the Netherlands Organization for Scientific Research (NWO; grant number 024.003.013).

Authors' contributions

LL, LG, SW, and AC designed the study. LL and PA performed the literature review. LL conducted the sensitivity analyses, full-model simulations, and model validation. JM, SW, and AC developed and analyzed the early-healing submodel. LL drafted the

manuscript, except for the early-healing submodel sections, which were drafted by JM and SW. All authors revised the manuscript, with revisions implemented by LL. Figures were prepared by LL (Figs. 1–3, 6–8) and SW (Figs. 4–5). LG, SW, and AC supervised the project. All authors read and approved the final manuscript.

Acknowledgments

The authors thank the Banff International Research Station (BIRS) for Mathematical Innovation and Discovery for hosting and funding the workshop "Sex Differences in Physiology: Mathematical Modelling and Analysis" (23w5045) in which this study started. For the purpose of open access, the authors have applied a CC BY public copyright license to any author accepted manuscript arising from this submission.

Supplementary information

This article has an accompanying supplementary file providing details on the literature-guided sex-specific parameterization, sensitivity analyses, and quantitative results from the full model.

References

[1] Zura, R., Xiong, Z., Einhorn, T., Watson, J.T., Ostrum, R.F., Prayson, M.J., Rocca, G.J.D., Mehta, S., McKinley, T., Wang, Z., Steen, R.G.: Epidemiology of fracture nonunion in 18 human bones. JAMA Surgery **151** (2016) https://doi.org/10.1001/jamasurg.2016.2775

[2] Mills, L.A., Aitken, S.A., Simpson, A.H.R.W.: The risk of non-union per fracture: current myths and revised figures from a population of over 4 million adults. Acta Orthopaedica **88**(4), 434–439 (2017) https://doi.org/10.1080/17453674.2017.1321351

[3] Duda, G.N., Geissler, S., Checa, S., Tsitsilonis, S., Petersen, A., Schmidt-Bleek, K.: The decisive early phase of bone regeneration. Nature Reviews Rheumatology **19**(2), 78–95 (2023) https://doi.org/10.1038/s41584-022-00887-0

[4] Ekegren, C.L., Edwards, E.R., Steiger, R., Gabbe, B.J.: Incidence, costs and predictors of non-union, delayed union and mal-union following long bone fracture. International Journal of Environmental Research and Public Health **15** (2018) https://doi.org/10.3390/ijerph15122845

[5] Borgström, F., Karlsson, L., Ortsäter, G., Norton, N., Halbout, P., Cooper, C., Lorentzon, M., McCloskey, E.V., Harvey, N.C., Javaid, M.K., Kanis, J.A.: Fragility fractures in europe: burden, management and opportunities. Archives of Osteoporosis **15**, 59 (2020) https://doi.org/10.1007/s11657-020-0706-y

[6] Wildemann, B., Ignatius, A., Leung, F., Taitsman, L.A., Smith, R.M., Pesántez, R., Stoddart, M.J., Richards, R.G., Jupiter, J.B.: Non-union bone

fractures. Nature Reviews Disease Primers **7** (2021) https://doi.org/10.1038/s41572-021-00289-8

[7] Shansky, R.M., Murphy, A.Z.: Considering sex as a biological variable will require a global shift in science culture. Nature Neuroscience **24**, 457–464 (2021) https://doi.org/10.1038/s41593-021-00806-8

[8] Molitoris, K.H., Balu, A.R., Huang, M., Baht, G.S.: The impact of age and sex on the inflammatory response during bone fracture healing. JBMR Plus (2024) https://doi.org/10.1093/jbmrpl/ziae023

[9] Ueno, M., Zhang, N., Hirata, H., Barati, D., Utsunomiya, T., Shen, H., Lin, T., Maruyama, M., Huang, E., Yao, Z., Wu, J.Y., Zwingenberger, S., Yang, F., Goodman, S.B.: Sex differences in mesenchymal stem cell therapy with gelatin-based microribbon hydrogels in a murine long bone critical-size defect model. Frontiers in Bioengineering and Biotechnology **9** (2021) https://doi.org/10.3389/fbioe.2021.755964

[10] Kurapaty, S.S., Hsu, W.K.: Sex-based difference in bone healing: A review of recent pre-clinical literature. Current Reviews in Musculoskeletal Medicine **15**, 651–658 (2022) https://doi.org/10.1007/s12178-022-09803-1

[11] Toya, M., Kushioka, J., Shen, H., Utsunomiya, T., Hirata, H., Tsubosaka, M., Gao, Q., Chow, S.K.-H., Zhang, N., Goodman, S.B.: Sex differences of nf-κb-targeted therapy for mitigating osteoporosis associated with chronic inflammation of bone. Bone Joint Res **13**, 28–39 (2024) https://doi.org/10.1302/2046-3758

[12] Haffner-Luntzer, M., Fischer, V., Ignatius, A.: Differences in fracture healing between female and male c57bl/6j mice. Frontiers in Physiology **12** (2021) https://doi.org/10.3389/fphys.2021.712494

[13] Andrew, T.W., Koepke, L.S., Wang, Y., Lopez, M., Steininger, H., Struck, D., Boyko, T., Ambrosi, T.H., Tong, X., Sun, Y., Gulati, G.S., Murphy, M.P., Marecic, O., Telvin, R., Schallmoser, K., Strunk, D., Seita, J., Goodman, S.B., Yang, F., Longaker, M.T., Yang, G.P., Chan, C.K.F.: Sexually dimorphic estrogen sensing in skeletal stem cells controls skeletal regeneration. Nature Communications **13** (2022) https://doi.org/10.1038/s41467-022-34063-5

[14] Ortona, E., Pagano, M.T., Capossela, L., Malorni, W.: The role of sex differences in bone health and healing. Biology **12** (2023) https://doi.org/10.3390/biology12070993

[15] Nathan, K., Lu, L.Y., Lin, T., Pajarinen, J., Jämsen, E., Huang, J.-F., Romero-Lopez, M., Maruyama, M., Kohno, Y., Yao, Z., *et al.*: Precise immunomodulation of the m1 to m2 macrophage transition enhances mesenchymal stem cell osteogenesis and differs by sex. Bone & joint research **8**(10), 481–488 (2019) https://doi.org/10.1302/20463758.810

[16] Einhorn, T.A.: The cell and molecular biology of fracture healing. Clinical Orthopaedics and Related Research **355**, 7–21 (1998) https://doi.org/10.1097/00003086-199810001-00003

[17] Loi, F., Córdova, L.A., Pajarinen, J., Lin, T., Yao, Z., Goodman, S.B.: Inflammation, fracture and bone repair. Bone **86**, 119–130 (2016) https://doi.org/10.1016/j.bone.2016.02.020

[18] Harwood, P.J., Newman, J.B., Michael, A.L.: (ii) an update on fracture healing and non-union. Orthopaedics and Trauma **24**(1), 9–23 (2010) https://doi.org/10.1016/j.mporth.2009.12.004

[19] Claes, L., Recknagel, S., Ignatius, A.: Fracture healing under healthy and inflammatory conditions. Nature Reviews Rheumatology **8**(3), 133–143 (2012) https://doi.org/10.1038/nrrheum.2012.1

[20] Marsell, R., Einhorn, T.A.: The biology of fracture healing. Injury **42**(6), 551–555 (2011) https://doi.org/10.1016/j.injury.2011.03.031

[21] Lafuente-Gracia, L., Borgiani, E., Nasello, G., Geris, L.: Towards in silico models of the inflammatory response in bone fracture healing. Frontiers in Bioengineering and Biotechnology **9**, 703725 (2021) https://doi.org/10.3389/fbioe.2021.703725

[22] Zhang, T., Yao, Y.: Effects of inflammatory cytokines on bone/cartilage repair. Journal of Cellular Biochemistry **120**(5), 6841–6850 (2018) https://doi.org/10.1002/jcb.27953

[23] Maruyama, M., Rhee, C., Utsunomiya, T., Zhang, N., Ueno, M., Yao, Z., Goodman, S.B.: Modulation of the Inflammatory Response and Bone Healing. Frontiers in Endocrinology **11** (2020) https://doi.org/10.3389/fendo.2020.00386

[24] Horwood, N.J.: Macrophage polarization and bone formation: A review. Clinical Reviews in Allergy and Immunology **51**, 79–86 (2016) https://doi.org/10.1007/s12016-015-8519-2

[25] Pajarinen, J., Lin, T., Gibon, E., Kohno, Y., Maruyama, M., Nathan, K., Lu, L., Yao, Z., Goodman, S.B.: Mesenchymal stem cell-macrophage crosstalk and bone healing. Biomaterials **196**, 80–89 (2019) https://doi.org/10.1016/j.biomaterials.2017.12.025

[26] Tsiridis, E., Upadhyay, N., Giannoudis, P.: Molecular aspects of fracture healing: Which are the important molecules? Injury **38**(1, Supplement), 11–25 (2007) https://doi.org/10.1016/j.injury.2007.02.006

[27] Hart, D.A.: Regulation of bone by mechanical loading, sex hormones, and nerves: Integration of such regulatory complexity and implications for bone loss during space flight and post-menopausal osteoporosis. Biomolecules **13** (2023) https:

//doi.org/10.3390/biom13071136

[28] Allen, J.B., Ludtka, C., James, B.D.: Sex as a biological variable in tissue engineering and regenerative medicine. Annual Review of Biomedical Engineering **25**, 311–331 (2023) https://doi.org/10.1146/annurev-bioeng-092222

[29] Meszaros, L.B., Usas, A., Cooper, G.M., Huard, J.: Effect of host sex and sex hormones on muscle-derived stem cell-mediated bone formation and defect healing. Tissue Engineering - Part A **18**, 1751–1759 (2012) https://doi.org/10.1089/ten.tea.2011.0448

[30] Klein, S.L., Flanagan, K.L.: Sex differences in immune responses. Nature Reviews Immunology **16**, 626–638 (2016) https://doi.org/10.1038/nri.2016.90

[31] Carp, D.M., Liang, Y.: Universal or personalized mesenchymal stem cell therapies: Impact of age, sex, and biological source. Cells **11**(13) (2022) https://doi.org/10.3390/cells11132077

[32] Pennell, L.M., Galligan, C.L., Fish, E.N.: Sex affects immunity. Journal of Autoimmunity **38** (2012) https://doi.org/10.1016/j.jaut.2011.11.013

[33] Schneider, C.P., Schwacha, M.G., Chaudry, I.H.: Impact of sex and age on bone marrow immune responses in a murine model of trauma-hemorrhage. J Appl Physiol **102**, 113–121 (2007) https://doi.org/10.1152/japplphysiol.00848.2006

[34] Kher, A., Wang, M., Tsai, B.M., Pitcher, J.M., Greenbaum, E.S., Nagy, R.D., Patel, K.M., Wairiuko, G.M., Markel, T.A., Meldrum, D.R.: Sex differences in the myocardial inflammatory response to acute injury. Shock **23**, 1–10 (2005) https://doi.org/10.1097/01.shk.0000148055.12387.15

[35] Crisostomo, P.R., Wang, M., Herring, C.M., Markel, T.A., Meldrum, K.K., Lillemoe, K.D., Meldrum, D.R.: Gender differences in injury induced mesenchymal stem cell apoptosis and vegf, tnf, il-6 expression: Role of the 55 kda tnf receptor (tnfr1). Journal of Molecular and Cellular Cardiology **42**, 142–149 (2007) https://doi.org/10.1016/j.yjmcc.2006.09.016

[36] Mckinnirey, F., Herbert, B., Vesey, G., McCracken, S.: Immune modulation via adipose derived mesenchymal stem cells is driven by donor sex in vitro. Scientific Reports **11** (2021) https://doi.org/10.1038/s41598-021-91870-4

[37] Maged, G., Abdelsamed, M.A., Wang, H., Lotfy, A.: The potency of mesenchymal stem/stromal cells: does donor sex matter? Stem Cell Research & Therapy **15**(1), 112 (2024) https://doi.org/10.1186/s13287-024-03722-3

[38] Katsara, O., Mahaira, L.G., Iliopoulou, E.G., Moustaki, A., Antsaklis, A., Loutradis, D., Stefanidis, K., Baxevanis, C.N., Papamichail, M., Perez, S.A.: Effects of donor age, gender, and in vitro cellular aging on the phenotypic,

functional, and molecular characteristics of mouse bone marrow-derived mesenchymal stem cells. Stem Cells and Development **20**, 1549–1561 (2011) https://doi.org/10.1089/scd.2010.0280

[39] Sui, B.D., Chen, J., Zhang, X.Y., He, T., Zhao, P., Zheng, C.X., Li, M., Hu, C.H., Jin, Y.: Gender-independent efficacy of mesenchymal stem cell therapy in sex hormone-deficient bone loss via immunosuppression and resident stem cell recovery. Experimental and Molecular Medicine **50** (2018) https://doi.org/10.1038/s12276-018-0192-0

[40] Strube, P., Mehta, M., Baerenwaldt, A., Trippens, J., Wilson, C.J., Ode, A., Perka, C., Duda, G.N., Kasper, G.: Sex-specific compromised bone healing in female rats might be associated with a decrease in mesenchymal stem cell quantity. Bone **45**, 1065–1072 (2009) https://doi.org/10.1016/j.bone.2009.08.005

[41] Zhang, H., Kot, A., Lay, Y.A.E., Fierro, F.A., Chen, H., Lane, N.E., Yao, W.: Acceleration of fracture healing by overexpression of basic fibroblast growth factor in the mesenchymal stromal cells. Stem Cells Translational Medicine **6**, 1880–1893 (2017) https://doi.org/10.1002/sctm.17-0039

[42] Decoene, I., Svitina, H., Belal Hamed, M., Economou, A., Stegen, S., Luyten, F.P., Papantoniou, I.: Callus organoids reveal distinct cartilage to bone transition mechanisms across donors and a role for biological sex. Bone Research **13**(1), 41 (2025) https://doi.org/10.1038/s41413-025-00418-z

[43] Seeman, E.: The structural and biomechanical basis of the gain and loss of bone strength in women and men. Endocrinology and Metabolism Clinics of North America **32**(1), 25–38 (2003) https://doi.org/10.1016/S0889-8529(02)00078-6

[44] Ko, C.-Y., Hyun Seo, D., Sung Kim, H.: Deterioration of bone quality in the tibia and fibula in growing mice during skeletal unloading: Gender-related differences. Journal of Biomechanical Engineering **133**(11), 111003 (2011) https://doi.org/10.1115/1.4005350

[45] Patel, S., Baker, L., Perez, J., Vulcano, E., Kaplan, J., Aiyer, A.: Risk factors for nonunion following ankle arthrodesis: A systematic review and meta-analysis. Foot and Ankle Specialist **16**, 60–77 (2023) https://doi.org/10.1177/1938640021998493

[46] Jensen, S.S., Jensen, N.M., Gundtoft, P.H., Kold, S., Zura, R., Viberg, B.: Risk factors for nonunion following surgically managed, traumatic, diaphyseal fractures: a systematic review and meta-analysis. EFORT Open Reviews **7**, 516–525 (2022) https://doi.org/10.1530/EOR-21-0137

[47] Sanchez, G., Vargas, M., Gordon, A.M., Golub, I., Ashraf, A., Diamond, K., Kang, K.K., Razi, A.E.: Risk factors for nonunion following open reduction and internal fixation for proximal humerus fractures. European Journal of

Orthopaedic Surgery and Traumatology **33**, 883–888 (2023) https://doi.org/10.1007/s00590-022-03221-2

[48] Saul, D., Menger, M.M., Ehnert, S., Nüssler, A.K., Histing, T., Laschke, M.W.: Bone healing gone wrong: Pathological fracture healing and non-unions—overview of basic and clinical aspects and systematic review of risk factors. Bioengineering **10** (2023) https://doi.org/10.3390/bioengineering10010085

[49] Doblaré, M., García, J.M., Gómez, M.J.: Modelling bone tissue fracture and healing: A review. Engineering Fracture Mechanics **71**(13-14), 1809–1840 (2004) https://doi.org/10.1016/j.engfracmech.2003.08.003

[50] Carlier, A., Geris, L., Lammens, J., Van Oosterwyck, H.: Bringing computational models of bone regeneration to the clinic. Wiley Interdisciplinary Reviews: Systems Biology and Medicine **7**(4), 183–194 (2015) https://doi.org/10.1002/wsbm.1299

[51] Giorgi, M., Verbruggen, S.W., Lacroix, D.: In silico bone mechanobiology: modeling a multifaceted biological system. Wiley Interdisciplinary Reviews: Systems Biology and Medicine **8**(6), 485–505 (2016) https://doi.org/10.1002/wsbm.1356

[52] Borgiani, E., Duda, G.N., Checa, S.: Multiscale Modeling of Bone Healing: Toward a Systems Biology Approach. Frontiers in Physiology **8**, 287 (2017) https://doi.org/10.3389/fphys.2017.00287

[53] Ghiasi, M.S., Chen, J., Vaziri, A., Rodriguez, E.K., Nazarian, A.: Bone fracture healing in mechanobiological modeling: A review of principles and methods. Bone Reports **6**, 87–100 (2017) https://doi.org/10.1016/j.bonr.2017.03.002

[54] Wang, M., Yang, N., Wang, X.: A review of computational models of bone fracture healing. Medical and Biological Engineering and Computing **55**, 1895–1914 (2017) https://doi.org/10.1007/s11517-017-1701-3

[55] Wang, M., Jiang, G., Yang, H., Jin, X.: Computational models of bone fracture healing and applications: a review. Biomedical Engineering / Biomedizinische Technik **69**(3), 219–239 (2024) https://doi.org/10.1515/bmt-2023-0088

[56] Kojouharov, H.V., Trejo, I., Chen-Charpentier, B.M.: Modeling the effects of inflammation in bone fracture healing. AIP Conference Proceedings **1895**(1), 020005 (2017) https://doi.org/10.1063/1.5007359 https://aip.scitation.org/doi/pdf/10.1063/1.5007359

[57] Trejo, I., Kojouharov, H., Chen-Charpentier, B.: Modeling the Macrophage-Mediated Inflammation Involved in the Bone Fracture Healing Process. Mathematical and Computational Applications **24**(1), 12 (2019) https://doi.org/10.3390/mca24010012

[58] Trejo, I., Kojouharov, H.: A mathematical model to study the fundamental functions of phagocytes and inflammatory cytokines during the bone fracture healing process. Letters in Biomathematics **7**(1), 171–189 (2020)

[59] Baratchart, E., Lo, C.H., Lynch, C.C., Basanta, D.: Integrated computational and in vivo models reveal key insights into macrophage behavior during bone healing. PLOS Computational Biology **18**(5), 1009839 (2022)

[60] Borgiani, E., Nasello, G., Ory, L., Herpelinck, T., Groeneveldt, L., Bucher, C.H., Schmidt-Bleek, K., Geris, L.: Commbini: an experimentally-informed computational model of macrophage dynamics in the bone injury immunoresponse. Frontiers in Immunology **14**, 1231329 (2023)

[61] Yu, T.: Design and validation of a mathematical model to describe macrophage dynamics in wound healing. PhD thesis, Drexel University (August 2014). https://doi.org/10.17918/etd-6080

[62] Wang, Y., Yang, T., Ma, Y., Halade, G.V., Zhang, J., Lindsey, M.L., Jin, Y.F.: Mathematical modeling and stability analysis of macrophage activation in left ventricular remodeling post-myocardial infarction. BMC genomics **13 Suppl 6** (2012) https://doi.org/10.1186/1471-2164-13-s6-s21

[63] Sobol, I.M.: Global sensitivity indices for nonlinear mathematical models and their monte carlo estimates. Mathematics and computers in simulation **55**(1-3), 271–280 (2001)

[64] Saltelli, A., Ratto, M., Andres, T., Campolongo, F., Cariboni, J., Gatelli, D., Saisana, M., Tarantola, S.: Global Sensitivity Analysis: the Primer. John Wiley & Sons, ??? (2008)

[65] Haffner-Luntzer, M., Kovtun, A., Rapp, A.E., Ignatius, A.: Mouse models in bone fracture healing research. Current Molecular Biology Reports **2**(2), 101–111 (2016)

[66] Koh, N.Y., Miszkiewicz, J.J., Fac, M.L., Wee, N.K., Sims, N.A.: Preclinical rodent models for human bone disease, including a focus on cortical bone. Endocrine Reviews **45**(4), 493–520 (2024)

[67] R Core Team: R: A Language and Environment for Statistical Computing. R Foundation for Statistical Computing, Vienna, Austria (2021). R Foundation for Statistical Computing. https://www.R-project.org/

[68] Birkhold, A.I., Razi, H., Duda, G.N., Weinkamer, R., Checa, S., Willie, B.M.: The influence of age on adaptive bone formation and bone resorption. Biomaterials **35**(34), 9290–9301 (2014) https://doi.org/10.1016/j.biomaterials.2014.07.051

[69] Razi, H., Birkhold, A.I., Weinkamer, R., Duda, G.N., Willie, B.M., Checa,

S.: Aging leads to a dysregulation in mechanically driven bone formation and resorption. Journal of Bone and Mineral Research **30**(10), 1864–1873 (2015)

[70] Borgiani, E., Figge, C., Kruck, B., Willie, B.M., Duda, G.N., Checa, S.: Age-Related Changes in the Mechanical Regulation of Bone Healing Are Explained by Altered Cellular Mechanoresponse. Journal of Bone and Mineral Research **34**(10), 1923–1937 (2019) https://doi.org/10.1002/jbmr.3801

[71] Tosi, L.L., Boyan, B.D., Boskey, A.L.: Does sex matter in musculoskeletal health?: The influence of sex and gender on musculoskeletal health. JBJS **87**(7), 1631–1647 (2005)

[72] Winter, E.M., Ireland, A., Butterfield, N.C., Haffner-Luntzer, M., Horcajada, M.-N., Veldhuis-Vlug, A., Oei, L., Colaianni, G., Bonnet, N.: Pregnancy and lactation, a challenge for the skeleton. Endocrine connections **9**(6), 143–157 (2020) https://doi.org/10.1530/EC-20-0055

[73] Beery, A.K., Zucker, I.: Sex bias in neuroscience and biomedical research. Neuroscience and Biobehavioral Reviews **35**, 565–572 (2011) https://doi.org/10.1016/j.neubiorev.2010.07.002

[74] Yoon, D.Y., Mansukhani, N.A., Stubbs, V.C., Helenowski, I.B., Woodruff, T.K., Kibbe, M.R.: Sex bias exists in basic science and translational surgical research. Surgery (United States) **156**, 508–516 (2014) https://doi.org/10.1016/j.surg.2014.07.001

[75] Plevkova, J., Brozmanova, M., Harsanyiova, J., Sterusky, M., Honetschlager, J., Buday, T.: Various aspects of sex and gender bias in biomedical research. Physiological Research **69**, 367–378 (2021) https://doi.org/10.33549/PHYSIOLRES.934593

Supplementary Files

This is a list of supplementary files associated with this preprint. Click to download.

- SupplementaryMaterial.pdf